

© 2021 by Zoë Richter. All rights reserved.

—

BY

ZOË RICHTER

THESIS

Submitted in partial fulfillment of the requirements
for the degree of Master of Science in Nuclear, Plasma, Radiological Engineering
in the Graduate College of the
University of Illinois at Urbana-Champaign, 2021

Urbana, Illinois

Master's Committee:

—

Abstract

Acknowledgments

Acks.

Table of Contents

List of Tables	v
List of Figures	vi
Chapter 1 Introduction	1
1.1 Motivation	1
1.2 Objectives	2
1.3 Background	2
1.3.1 The High Temperature Gas Cooled Reactor: Beginnings and Concepts	2
1.3.2 Earliest Operational HTGRs	4
1.3.3 Serpent	7
Chapter 2 Literature Review	8
2.1 Computational Models	8
2.1.1 Serpent	8
2.1.2 Work in Other Software	8
2.1.3 Fuel Modeling	9
2.2 Modern HTGRs	10
2.2.1 PBMR	10
2.2.2 Next Generation Nuclear Plant (NGNP)	12
2.2.3 X-energy	12
Chapter 3 Methodology	13
3.1 Sangamon200	15
3.2 Sangamon20	16
3.2.1 Inner Core Volume Determination	16
3.2.2 Graphite Reflector Thickness Determination	18
3.3 Fuel Composition	18
3.4 Reactor Sensitivity to Pebble Locations and Symmetry	19
Chapter 4 Results	21
4.1 Fuel Isotopic Compositions	21
4.2 Full-Core Control Model	23
4.3 Effect of Homogenizing	28
4.4 Sensitivity Tests	33
4.4.1 Effects of Symmetry Assumption	33
4.4.2 Effects of Pebble Shuffling	35
Chapter 5 Conclusion	41
References	43

List of Tables

3.1	Reactor Parameters: Sangamon200 and Sangamon20	13
3.2	Pebble Parameters	14
3.3	Particle Parameters	14
4.1	Run Summary	33
4.2	Run Summary	36

List of Figures

1.1 Side-View of the 1955 Daniels' Concept, [1]	3
1.2 Diagram of Coolant Flow in the 1955 Daniel's Concept, [1]	3
1.3 Helium Coolant Specific Activities [3]	6
1.4 Pebble Dust Specific Activities [3]	7
2.1 PBMR Schematic: Vertical Cross-section [5]	11
3.1 Pebble Zones	14
3.2 TRISO Particle Layers (not to scale)	15
3.3 Detector Placement Inside Reflector	16
3.4 Curve of Possible Height and Radii by Packing Fraction	18
3.5 Geometry of the Single-Pebble Burnup Calculation: Sangamon20	19
3.6 Symmetry Test Run Layouts	20
4.1 Mesh Figures For Single Pebble Burnup	22
4.2 Evolution of Certain Isotopic Concentrations in Pebbles over Six Six-Month Passes	23
4.3 Legend for Geometry Figures	24
4.4 Full Core	25
4.5 Radial Thermal and Fast Flux Profiles	26
4.6 Axial Thermal and Fast Flux Profiles	26
4.7 Thermal and Fast Flux Profiles	27
4.8 Lethargy Adjusted Neutron Flux Energy Spectra	27
4.9 Full Core Using Heterogenized Pebbles	29
4.10 Radial Thermal and Fast Flux Profiles: Heterogenized Pebbles	30
4.11 Axial Thermal and Fast Flux Profiles: Heterogenized Pebbles	30
4.12 Thermal and Fast Flux Profiles	30
4.13 Lethargy Adjusted Neutron Flux Energy Spectra: Core Using Heterogenized Pebbles	31
4.14 Relative Difference in Radial Thermal and Fast Flux Profiles Between Cores Using Homogenized and Heterogenized Pebbles	31
4.15 Relative Difference in Lethargy Adjusted Neutron Flux Energy Spectra Between Cores using Homogenized and Heterogenized Pebbles	32
4.16 Sensitivity Analysis: $0^\circ - 60^\circ$	34
4.17 An Image Generated by Subtracting 4.16b from 4.17.	35
4.18 Sensitivity Analysis: $60^\circ - 120^\circ$	36
4.19 Sensitivity Analysis: $120^\circ - 180^\circ$	37
4.20 Sensitivity Analysis: $180^\circ - 240^\circ$	38
4.21 Sensitivity Analysis: $240^\circ - 300^\circ$	39
4.22 Sensitivity Analysis: $300^\circ - 360^\circ$	40

Chapter 1

Introduction

1.1 Motivation

The effects of global warming are becoming increasingly severe. (**include NASA facts?**). In the interest of reducing the global carbon footprint, a desire for carbon-free, sustainable energy is growing. With this interest comes a bevy of new research in the next generation of nuclear reactors.

One such class of reactors are the high temperature gas-cooled reactor, or HTGR. While HTGRs can have a variety of fuel forms, of particular interest are pebble bed reactors. A pebble-type fuel generally consists of a sphere of graphite, approximately the size of a billiard ball, embedded with TRISO particles. The fuel kernels in these TRISO particles are surrounded in multiple layers of carbon and silicon carbide, and, along with the graphite that creates the sphere proper, form a durable, compact fuel form. In addition, the pebbles are able to be refueled online, reducing the need for planned shutdowns.

The next generation of nuclear reactors also include designs significantly smaller than the conventional Light Water Reactor(LWR) seen in the USA today. So-called Small Modular Reactors, or SMRs, these reactors are small enough to be shipped, reactor pressure vessel and all, in a standard shipping truck or train. The pressure vessels can also be produced in a factory of standard size (**** I dislike this wording. but can't think of another way to put it****). SMRs can be deployed in a variety of new settings, such as isolated towns or work sites, or many can be stationed together in one plant to fill the role of a single larger reactor.

This work used a pebble-bed HTG-SMR as a starting point, and modeled a fairly generic 200MWth reactor based on existing designs - named Sangamon200. Then it scaled down to a target size - a 20MWth pebble bed HTGR. "Microreactors" such as these are generally 70 MWth or less, and can be deployed in areas where only a small amount of power is needed, used for research and testing, or be used to supply heat for other industrial processes, such as producing hydrogen.

Down-sized modular reactors, such as SMRs or microreactors, have a few inherent safety benefits over their larger cousins, which also prompts their development. The smaller scale of the reactor pressure vessel (RPV) makes the large active cooling loops of contemporary commercial nuclear reactors unnecessary. For smaller reactors,

decay heat can be removed with passive systems that rely on natural convection and surface heat transfer after something such as a station black-out (SBO). When power is supplied, supplementary fans and surface coolers can aid heat removal [29].

The 20MWth model, which will hereafter be referred to as Sangamon20, is of a highly simplified design, which can be used in future testing and analysis.

1.2 Objectives

This work briefly describes a 200 MWth pebble-bed HTGR SMR, inspired by concepts from the PBMR and X-energy reactors, henceforth named Sangamon200. After establishing the larger model as a baseline, a scaled-down 20 MWth model, Sangamon20, is designed, and is the focus of this work.

Using Sangamon20, a variety of modifications to its model are made, and their effects on key parameters are investigated. These modifications include heterogenizing versus homogenizing the pebble centers, applying a 6-point symmetry to the core (using $\frac{1}{16}$ to approximate the entire core), and a simple test of re-assigning pebble fuel compositions to test the model's randomness and pebble mixing. Additionally, the isotopic compositions for all pebble burnups are supplied, and trends over increasing burnup are discussed.

1.3 Background

1.3.1 The High Temperature Gas Cooled Reactor: Beginnings and Concepts

High temperature gas cooled reactors, or HTGRs, are one of the more commonly seen Generation IV reactor designs. It most often uses helium as a coolant, and graphite as a moderator in thermal designs. Fuel is in the form of tristructural-isotropic, or TRISO particles. TRISO particles use a small kernel of fuel, less than half a millimeter across, surrounded by layers of carbon and silicon carbide to protect the fuel kernel and prevent the leakage of radioisotopes ***(would it also be accurate to say the layers provide moderating material? I know that graphite is a great moderator, but I would think the main purpose is safety and to prevent leaching, and moderation is really in the graphite the particles are embedded in)***. These TRISO particles are then embedded in graphite to form a usable fuel element. In prismatic HTGRs, the graphite is in the shape of hexagonal columns. In pebble-bed reactors, the graphite is in the shape of spheres, around the size of a billiard ball. Many of these pebbles are loaded into the core, and slowly move through the bottom in a manner not dissimilar to grain in silos.

HTGRs, however, are not a new concept. Preliminary concepts for a gas-cooled reactor were created as early as 1942. Farrington Daniels - more commonly known for work in chemistry and solar power technology - is attributed

with establishing the first theoretical designs. A professor from the University of Wisconsin, Professor Daniel's work with Oak Ridge National Laboratory (ORNL) nailed-down the most basic characteristics of the HTGR. The choice of helium for coolant, graphite for moderator, the direct gas turbine cycle, and the use of uranium or thorium carbides for fuel all came from his work [1].

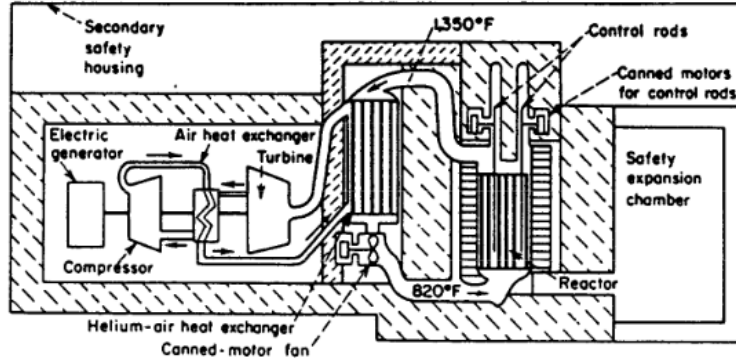


Figure 1.1: Side-View of the 1955 Daniels' Concept, [1]

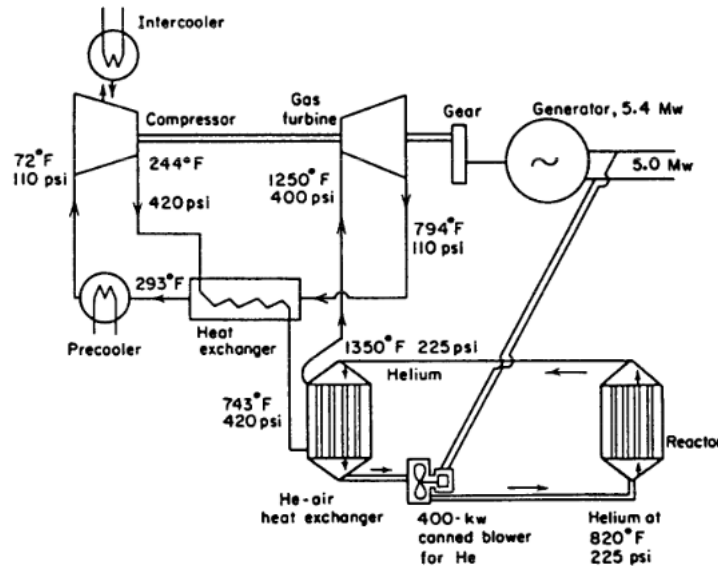


Figure 1.2: Diagram of Coolant Flow in the 1955 Daniel's Concept, [1]

Figures 1.1 and 1.2 show the design of the 1955 design proposed by Professor Daniels. Like many modern modular reactor plant designs, Professor Daniels suggested that the reactor be mostly underground. A key difference between the Farrington Daniels designs and modern HTGRs is the fuel form. While modern designs use TRISO particles embedded in graphite, the Daniels' design uses solid graphite blocks, with channels for both coolant and fuel. Within the fuel channels, fuel was loaded in either a pellet or cartridge form, both a mixture of 10% uranium dicarbide and graphite powder. In addition to these fuel channels, the design included an outer ring of graphite

reflector in which thorium was used to breed U-233. Control rods were made of boron-containing molybdenum. Additional safety rods made of the same were held above the core by steel wires that would melt in the case of an accident, dropping the safety rods into the core [1].

1.3.2 Earliest Operational HTGRs

The earliest operational HTGRs were first started in the 1960s. The AVR, from Germany, Dragon, operating in the UK, and Peach Bottom 1, which operated in the US [2].

Dragon

The Dragon prismatic HTGR was a test reactor operated in Winfrith, UK, from 1964 to 1975, making it the oldest of the reactors discussed in this chapter. It operated at inlet and outlet temperatures of 350°C and 750°C and a power of 20MWt [2]. Dragon's main purpose was to test reactor materials, with an emphasis on fuels. It originally used uranium and thorium as fuel, but switched to a purely uranium-based fuel with a lower enrichment later in life. The fuel elements themselves were similar in shape to the Daniels' design - hexagonal prisms with fuel rod channels.

Contrary to the fuel philosophy seen today, Dragon originally allowed fission products to be released from fuel elements into the circulating helium coolant. The fission products would then be purged from the helium. However, Dragon later switched to a coated-particle fuel when it became clear that having such large fission product releases would be difficult to manage [1].

Peach Bottom 1

Peach Bottom 1 operated from 1966 to 1974, by the Philadelphia Electric Company. It was the first operational HTGR in the US, and the first to produce electric power. It was slightly larger than Dragon, at a nameplate capacity of 115 MWt/40MWe and a slightly lower operating temperature range at 327°C to 700°C inlet to outlet [2]. Like Dragon, Peach Bottom 1 was a prismatic reactor, however, Peach Bottom used coated uranium and thorium carbide particles from the beginning. The original fuel used a single coating of pyrolytic carbon. However, after multiple fuel failures, Peach Bottom upgraded to bistructural isotropic, or BISO, fuels by adding an additional layer. Peach Bottom would later upgrade the fuel once again by adding a silicon carbide layer, forming TRISO particles [2]. One operational benefit of upgrading to TRISO particles from BISO particles was that the superior fission product retention meant that Peach Bottom 1 could remove the helium purging systems. In addition to the inner fuel region, Peach Bottom, like the Daniels' design, bred U-233 in an outer region using thorium.

Beyond changing the number and materials for fuel coatings, the experiences in Peach Bottom 1 helped to develop HTGR fuel elements. Operators saw that by using the graphite moderating material to dilute the fuel, the

fuel could be diluted further compared to other diluents. This of course has the advantage of saving fuel material, but also improved heat transfer and reduced radiation damage. Additionally, operational experience showed that, in order to prevent the creation and buildup of U-236 and Np-237, which are poisons, the U-235 and U-233 should be kept separate [1].

In the end, Peach Bottom 1 closed when it was determined to be uneconomical.

AVR

The Arbeitsgemeinschaft Versuchsreaktor (AVR) was an experimental pebble-bed reactor operated in the Jülich Research Center from 1967 to 1988. It had a capacity of 46 MWt/15MWe, with inlet and outlet temperatures of 275°C and 950°C [2]. In fact, the AVR reached the highest operating temperatures of any commercial nuclear plant. Like the others in this early time period, the AVR used a combination of uranium and thorium fuels, though the AVR began with BISO particles. The core held around 100,000 graphite pebbles, almost a third of which had fuel in them.

Despite not being built for experimental purposes, the AVR still housed many experiments that improved our body of knowledge in HTGR technology. During the first few years of its life, the goal of the AVR was to demonstrate that it was a reliable technology. After this initial period, the AVR could shift to allowing various experiments.

A step was to show that the reactor could operate safely, could control the core power and temperatures and safely shut down and remain sub-critical for long periods of time. This proved to be quite the undertaking, as the AVR shifted from highly enriched to low enriched fuel over time, which caused a large variety in fuel pebble compositions, on top of the range of compositions inherent to a multi-pass pebble cycle.

The AVR also provided data to validate models of pebble-bed reactors, and conducted an experiment to better characterize the radial distribution of temperatures in the core. A number of marked pebbles were loaded into the core, each housing a series of wires that would melt at a certain temperature, the lowest being 655°C, the highest 1280°C. The pebble positions were tracked based on pebble flow data, and when the spheres were ejected, they were examined to determine what temperatures the pebbles had experienced. Despite the outlet temperature being determined to be 950°C, multiple pebbles experienced a temperature greater than or equal to the 1280°C maximum temperature in the melt wires. It was noted that these pebbles went through a zone with a spike in local power density [3].

The AVR also demonstrated the inherent safety of HTGR reactors in accident scenarios by purposefully causing failure of active cooling system "accidents". In the first, the coolant blowers were shutoff, and no shutdown rods were inserted while operating at full power. The operators additionally shut the main circuit valves to prevent natural circulation to regions outside the active core. Overall, the changes to core temperatures were unremarkable. The hottest regions cooled, while the coldest regions warmed up. Additionally, due to negative temperature feedback

coefficients, the reactor power immediately declined in response to the "accident". The temperature slowly rose to 2 MW again over 24 hours, only to level out around 300 kW. A further test provided data on loss of coolant and depressurization accidents. As before, the core temperature changes were not particularly drastic. The upper core region was seen cooling, while the lower, originally cooler core region slowly rose in temperature. This experiment's data was used to validate HTGR computer models, which allowed the results to be aid in the analysis of other HTGRs [3].

Beyond accident safety, the AVR allowed for testing and demonstration of the safety qualities of TRISO and BISO fuel elements, especially relating to high temperature tolerance and fission product retention. Initial tests were conducted with BISO based pebbles, then later transitioned to TRISO, then low-enriched TRISO pebbles. The TRISO-LEU pebbles were shown to have good fission product retention compared to their BISO-based predecessors, based on the results of sampling the activity of the circulating helium to the presence of released fission products. Beyond radioisotopes being directly released into the coolant gas, the AVR also showed that in order to accurately characterize the source term of an HTGR pebble bed reactor, one must take the dust from the pebbles into account. Dust from the pebbles bumping and scraping against each other was found deposited on reactor surfaces in the primary loop. It was found that 60 kg of dust had accumulated by the end of the reactor's life, which averages to 3 kg of dust each year. Measurements of specific activity in the dust showed that the activities of Cs-137, Cs-134, I-131, Sr-90, and Co-60 were on the order of $10^6 \frac{\text{Bq}}{\text{g}}$. Even though there is relatively little dust, the activity of this dust is fairly high, especially compared to the activity of the coolant gas [3].

*** (I'm going to include here the two tables comparing the activities of the coolant gas and dust activities. However, the one for gas is (reasonably) by volume, while the dust is by mass. Should I use the density of helium at operating temperature to convert the gas activity to be in Bq/g, and make a new table (citing my source), or leave as-is?)***

Table 2
Specific activities of the primary coolant gas [Bq/m^3 (ISA)]

ΣFission noble gas	4.6×10^8
Tritium	3.7×10^7
C 14	1.9×10^7
Cs-137	3.0×10^2
I-131	5.2×10^2
Ag-110m	4.9×10^1
Sr-90	2.0×10^2
Co-60	1.0×10^1

Figure 1.3: Helium Coolant Specific Activities [3]

Table 3
Specific activities on dust [10^6 Bq/g]. The variation range results from measurements at different sampling locations and different times

Cs-137	2 – 96
Cs-134	0.7 – 27
I-131	0 – 3
Ag-110m	0.1 – 43
Sr-89	0.6 – 42
Sr-90	19 – 363
Co-60	0.2 – 8

Figure 1.4: Pebble Dust Specific Activities [3]

1.3.3 Serpent

Serpent 2 is "a multi-purpose three-dimensional continuous-energy Monte Carlo particle transport code" [4] from the VTT Technical Research Center of Finland. The first iteration, Serpent 1, began development in 2004. The development of Serpent 2 is presently ongoing. Serpent 2 has three main applications: traditional reactor physics, coupled multi-physics, and neutron and photon transport.

Chapter 2

Literature Review

2.1 Computational Models

While only Serpent 2.0 [10] is used in this thesis, work to improve HTGR modeling in one program can inform efforts in another. Therefore, modeling software beyond Serpent 2.0 is discussed in this chapter.

2.1.1 Serpent

In order to create and model complex geometries, Serpent uses constructive solid geometry (CSG), which defines homogeneous material cells using user-defined universes, cells, lattices, and specially-defined nested objects to define particle and pebble geometries. Using these special objects and the particle dispersal routine in Serpent, TRISO particles and pebble bed reactors can be modeled. Serpent has been tested with up to 60 million individual particles [4].

Physics are based on a combination of classical kinematics, ENDF reaction laws, and random sampling. For particle transport, Serpent uses surface tracking and Woodcock-delta tracking. For material data, Serpent uses ACE format libraries for microscopic cross sections, and pre-generates macroscopic cross sections before beginning transport. To further speed-up calculations, Serpent uses a unionized energy grid. Serpent has been validated against MCNP, and validation is ongoing for radiation shielding and criticality safety analysis. While the differences between Serpent and other Monte Carlo codes are usually marginal, Serpent experiences the same issues validating its results as other Monte Carlo programs, related to small differences in data libraries [4].

2.1.2 Work in Other Software

A 1996 effort to improve MCNP developed a new sampling method for Monte Carlo. The version of MCNP that used the sampling model was dubbed MCNP-BALL. After testing by performing isotopic inventory and criticality calculations , it was seen that the MCNP-BALL code could get results accurate to 0.2%. The work developing MCNP-BALL also answered a weakness in core modeling due related to difficulties in modeling reactors with a so-called "double-heterogeneity" - having two or more types of pebble in a single reactor [43].

An additional look into MCNP HTGR simulations examined the ability to model what would normally be a stochastic geometry with uniform modeling. Specifically, TRISO particles and pebbles were placed in body centered tetragonal BCT and hexagonal close pack (HCP). In general, it was found that for very low packing fractions, such as the values seen in TRISO-in-pebble packing, the particles are generally far enough away that the differences between two crystal lattice structures are insignificant. In smaller cores with adequate reflectors, the differences between the pebble packing lattices were more significant, but manageable. However, in unreflected cores and moderators that are not graphite, this is no longer true. Additionally, the effect of completely homogenizing the coating of the TRISO particles - blending them with the graphite matrix - caused a noticeable change, specifically lowering k_{eff} . For methods using less dramatic homogenization methods, such as blending the 4 TRISO coatings into one uniform layer, an appreciable decrease in computational load was observed, and the results were marginally different from the 4-coating model [46].

BEAU, or Burnup Equilibrium Analysis Utility [12], was developed to model depletion and multiple burnup states for a continuously refueled pebble bed reactor, using the multiple burnup state method (MBSM) to do so. MBSM improves on most full-core pebble bed computational methods by modeling all burnup states for a pebble, rather than homogenizing them into a representative average pebble.

BEAU is a python-based coupling software that combines either MCNP5 or Serpent with ORIGEN2, using new interface inspired by the MOCUP code named `mocup.py`. `Mocup.py` takes the output files from an MCNP5 or Serpent simulation, and compiles the information from the simulation into an object that can be used to run depletion simulations. BEAU can be used for fuel cycle analysis and finding the maximum burnup equilibrium. It has been bench-marked against results for a pebble-bed HTGR in INL's PEBBED and VSOP [12].

2.1.3 Fuel Modeling

BEAU was used to aid in the design of a pebble bed fluoride high temperature reactor, PB-FHR, named the Mark-1 PB-FHR [12]. Much of the analysis is beyond the scope of this thesis, however, the handling of pebble locations is of interest. The Mark-1 PB-FHR handles pebble locations using a face-centered cubic (FCC) lattice in which all burnup states seen in the reactor are present. If one assumes a uniformly mixed core, the closeness of the different burnup compositions in the lattice provide a fairly good estimation.

A more general study examined the effects of pebble packing on the core neutronics in an HTGR [45]. Rather than model a full core, a unit cell was created as a reference. The study considers body centered cubic (BCC) and hexagonal close-packed (HCP). Instead of using a variety of compositions to represent an equilibrium, middle-of-life (MOL) core, an enrichment of 9.6% - lower than the standard 15% for fresh HTGR pebble-fuel - is assumed for all pebbles. For each lattice configuration, the fuel/moderator (F/M) ratio was varied, and the effects on core

neutronics and isotopic compositions examined. No significant difference between BCC and HCP cells was found. The study determined it would likely be impossible to select a truly 'optimal' energy spectrum vis-à-vis minimizing the accumulation of particularly harmful fission products. The author concluded that F/M ratios less than 1/1 favor reducing actinide inventories, while ratios greater than 1/1 can reduce the generation of fission products that would corrode the layers of the TRISO fuel.

Earlier work on HTGRs by General Atomic determined the composition of discharged thorium/uranium prismatic fuel elements. This study assumes fuel recycling to complement the breed/burn fuel cycle proposed. Additionally, the fuel cycle assumes the reactor can start with an initial feed material of 93% U-235, which is not currently feasible (at least in commercial reactors in the United States) [48].

2.2 Modern HTGRs

The following discusses more recent HTGR designs, which are the inspiration for Sangamon200 and Sangamon20.

2.2.1 PBMR

The PBMR is a South African pebble bed HTGR design. While it did not ultimately make it to construction, its design has offered invaluable insight to later HTGR pebble bed designs. The PBMR is largely based on the German High Temperature Reactor (HTR) designs, and has a nameplate thermal power of 400 MW, with inlet-outlet temperatures of 500 °C to 900 °C. It is a modular design, with each unit containing a graphite moderated, helium-cooled core housed in a steel pressure vessel. In accident scenarios, the PBMR would rely on passive safety features using conduction and convection to provide cooling.

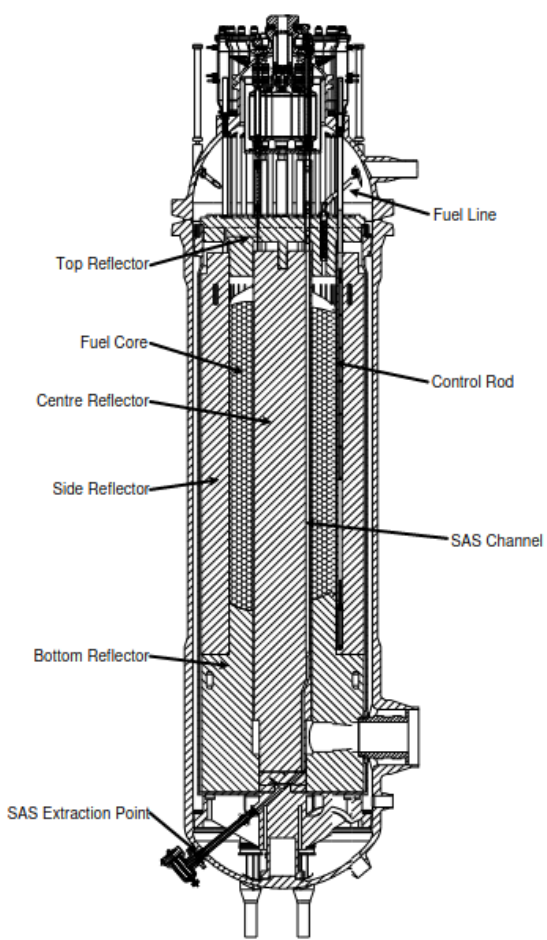


Figure 2.1: PBMR Schematic: Vertical Cross-section [5]

Each core unit would hold around half a million pebbles, which used LEU based TRISO particles as the fuel form. These TRISO particles are pressed into a 2.5cm radius graphite sphere, which then has an additional 0.5 cm thick layer of graphite pressed around it, to form a 3.0 cm radius pebble - around the size of a billiard ball. The pebbles would undergo a six-pass multi-pass cycle to reach a target end burnup of $92,000 \frac{MWd}{tU}$ [5].

2.2.2 Next Generation Nuclear Plant (NGNP)

Like the PBMR, the NGNP did not make it to construction. However, the work in analyzing reactor designs and materials is still applicable to other work. The NGNP project downselected its design choices to two models - a prismatic HTGR and a pebble-bed HTGR. While the NGNP project eventually opted for the Areva prismatic HTGR design [6] due to reasons related to pebble costs, it was noted that, technologically speaking, there was no inherent advantage or disadvantage between the two technologies [7].

Even though the reactor didn't make it to construction or operation, a plethora of research conducted in support of the NGNP project is applicable to similar reactors. One such study is a whole-core depletion study of the proposed prismatic HTGR design.

The reactor uses a once through fuel cycle, and assumed an average burnup of $100\text{-}150 \frac{GWd}{t}$ after an 18 to 24 month stint in the core. Much of the work from this study is applicable only to prismatic designs, namely the effects of the number of batches cycling, and fuel shuffling on core neutronics [44].

2.2.3 X-energy

Based on experience working on the PBMR project, the X-energy Xe-100 is a 200 MWt HTGR pebble-bed SMR. It is similar in design to all of its predecessors, featuring LEU TRISO particle fuel in 3.0 cm radius pebbles. While the Xe-100, or similar demonstration plant, has not been built as of this publication, the project is still ongoing. It is this reactor, and by extension, the PBMR, that the micro-reactor described in this thesis is most heavily influenced by.

The Xe-100 uses approximately 220,000 pebbles in a six-pass cycle, and fuel pebbles identical to the ones intended for the PBMR [8]. However, while the number of passes is the same, the target end burnup for the pebbles is higher, at $160,000 \frac{MWd}{tU}$ [9]. Another key difference from the PBMR beyond size is the lack of central reflector.

While the Xe-100 has not been built, there have been studies conducted by ORNL providing data on the production and material properties of the PBMR-type fuel pebble.

Chapter 3

Methodology

There are two reactor models created - Sangamon200, a 200MWth design inspired by the PBMR and Xe-100. Using data from the Sangamon200 model, a scaled down reactor called the Sangamon20 was created. Both are UCO-pebble fueled, helium cooled microreactors.

Parameter	Sangamon200	Sangamon20
Thermal Power [MW]	200	20
Average Core Temperature [K]	800K	800K
Enrichment	15.5%	19.75%
Average Core Pressure [MPa]	5.9	5.9
Core Diameter [cm]	248	180
Core Height [cm]	1150	180
Reflector Thickness [cm]	90	75
Number of Pebbles	220,000	23,000

Table 3.1: Reactor Parameters: Sangamon200 and Sangamon20

All simulations were performed using Serpent 2.0 [10]. Pebble and TRISO particle locations are both determined using the Serpent 2.0 particle dispersal routine. In Serpent 2.0, the particle dispersal algorithm first takes the number of particles, defined by the user directly, or indirectly using η_{pf} , the packing fraction, which is simply the total volume of particles in a space divided by the volume of that space. The dispersal routine also has the user define the particle radius, and the size and shape of the volume the particles are housed in. The routine first randomly determines a single point for each particle that is contained in the volume. Then, the routine uses the 'growth factor' and 'shake factor' - both described as fractions of the particle radius, and iterates. Each iteration, the size of the point's radius increases by the growth factor. Additionally, the center will move in a random direction a distance equal to the shake factor. If the particle growth would cause the particle to overlap with another particle or leave the volume, it doesn't get larger that cycle. Similarly, if the center's movement would cause overlap or leaving the containing volume, it doesn't move. The dispersal routine iterates until all particles are to their full size, contained in the volume, and do not overlap with any other particles. The routine generates an output file, where each line gives the coordinates of the particle center in x,y,z coordinates, the particle radius, and the name of the particle type, to associate it with the pbed card later.

In order to determine isotopic compositions in the pebbles, a Serpent burnup simulation of a single pebble is run in burnup steps of 180, 360, 540, 720, 900, and 1080 days - to represent 6, 6-month passes. A seventh composition is for a fresh pebble's composition. The single pebbles are the only models that utilize individually modeled TRISO particles. For the full-core models, each pebble is homogenized. Each pebble has two regions, an inner region that contains the TRISO particles embedded in graphite, and an outer region consisting only of graphite, see 3.1. Each region is homogenized by volume fraction using the mix card in Serpent.

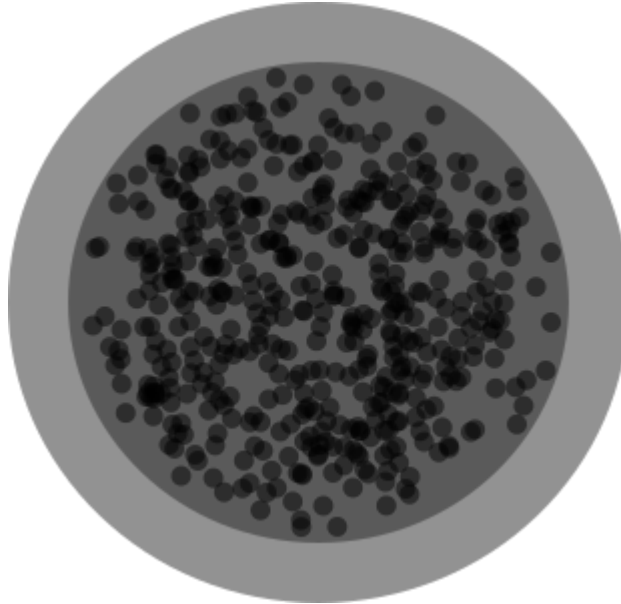


Figure 3.1: Pebble Zones

Parameter	Value
Fueled-Center Radius [cm]	2.5
Graphite Outer Shell Thickness [cm]	0.5cm
Total Radius [cm]	3.0
TRISO Particles per Pebble	18,000

Table 3.2: Pebble Parameters

Parameter	Value
Uranium Oxy carbide Kernel Radius [cm]	0.02125
Graphite Layer Thickness [cm]	0.03075
Inner Pyrolytic Carbon Layer Thickness [cm]	0.03475
Silicon Carbide Layer Thickness [cm]	0.03825
Outer Pyrolytic Carbon Layer Thickness [cm]	0.04225

Table 3.3: Particle Parameters

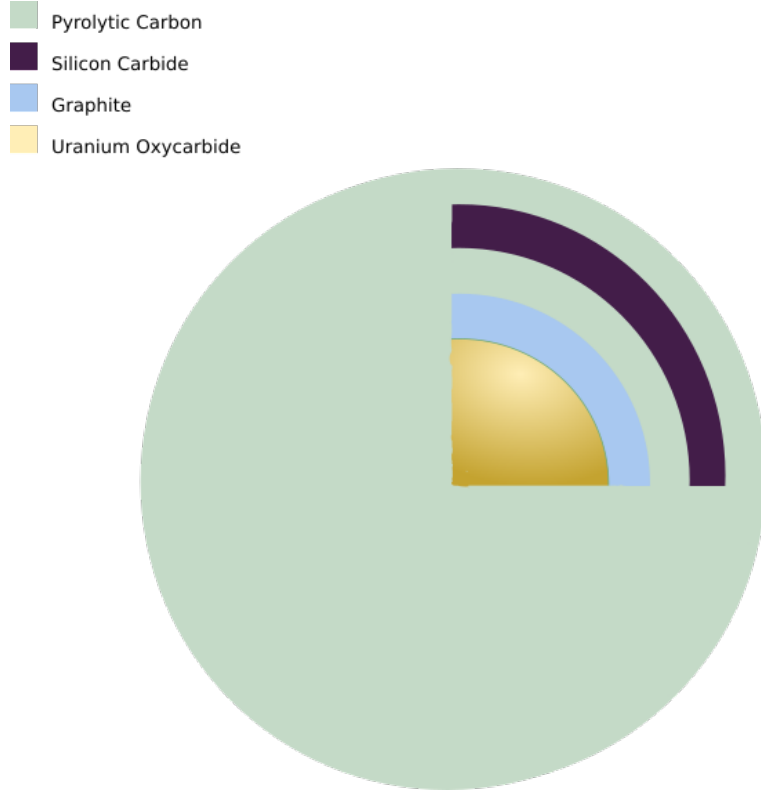


Figure 3.2: TRISO Particle Layers (not to scale)

3.1 Sangamon200

Sangamon200 is a 200 MWth helium cooled reactor, with parameters as defined in 3.1. Though the model does use some parameters from pre-established designs, it is still, a simplification. The "cone" formed at the top and bottom of the reactor core by the pebbles is averaged to a flat surface, to create a cylindrical core shape. The graphite reflector surrounds it, with no barriers between the reflector and helium/pebble-filled active core region. In effect, the reflector is the container for the pebbles. These are the only simulated parts of the reactor. It is assumed no control rods are being used. In addition, the graphite reflector is defined as a solid cylindrical shell.

While Sangamon200 is not the focus of this assessment, some neutronics features were determined to aid in Sangamon20's design. A surface current detector was placed in the reflector, just inside the outer bound of the reflector, as shown in 3.3.

This detector measures the outward neutron current (** serpent outputs units of [number/s], is current still the best word? ***) in [$\frac{\#}{s}$]. To arrive at the unit of [$\frac{\#}{cm^2 s}$] most are familiar with, the reported outward current is divided by the detector's surface area thus:

$$J^+ \left[\frac{\#}{cm^2 s} \right] = \frac{J^+ \left[\frac{\#}{s} \right]}{S_{det} [cm^2]} \quad (3.1)$$

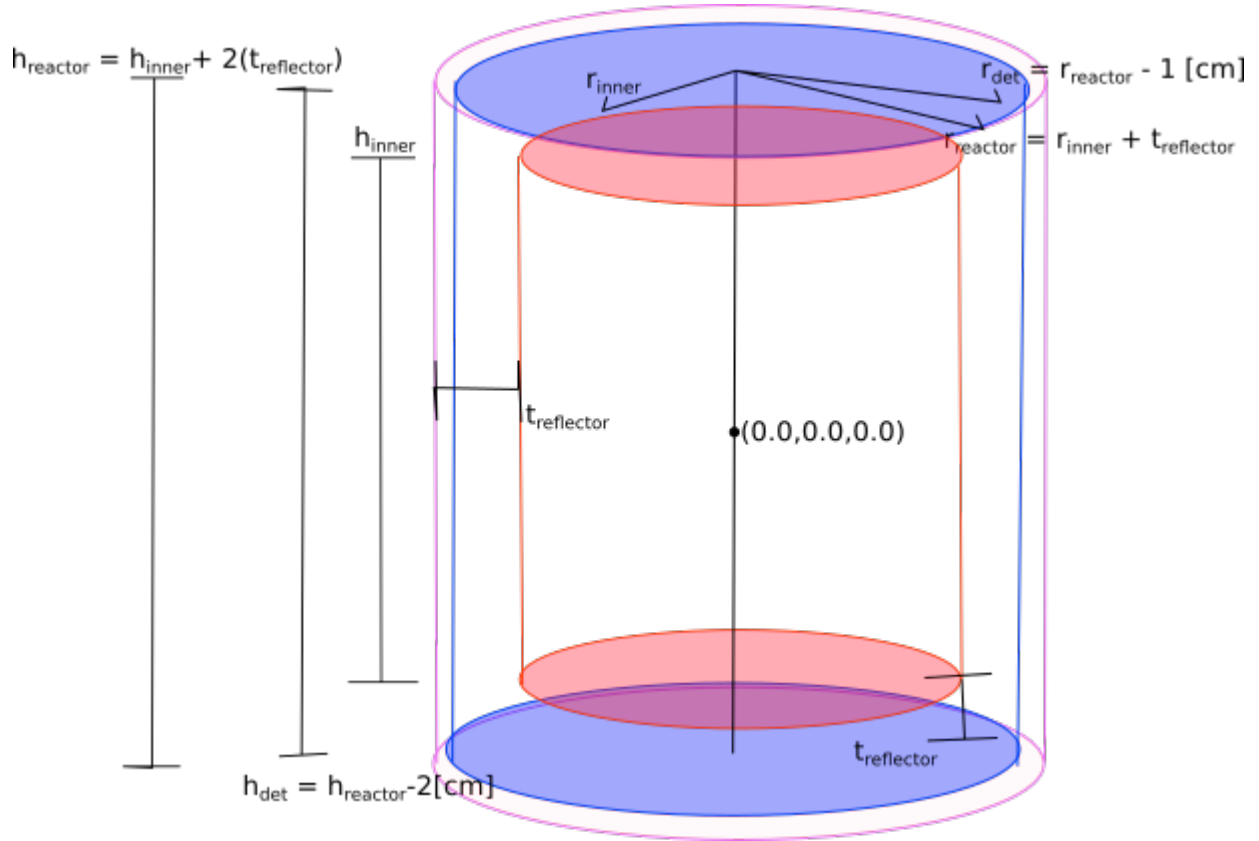


Figure 3.3: Detector Placement Inside Reflector

After accounting for the surface area, the outward current at the detector is 7.351×10^{11} .

3.2 Sangamon20

Sangamon20 is a 20 MWth helium-cooled pebble bed reactor, fueled with 19.75% enriched uranium oxycarbide. While the capacity of Sangamon20 is 10% that of Sangamon200, it isn't sufficient to simply scale Sangamon200's dimensions down to 10% of their original values, as that wouldn't have the correct volume for the required pebbles, and the neutronics wouldn't be preserved correctly.

3.2.1 Inner Core Volume Determination

The first assumption made in the scale-down is that Sangamon200 and Sangamon20 have the same power density, or $\frac{\text{kW}}{\text{g UCO}}$.

To calculate the mass of fuel in Sangamon200:

$$M_{f,200} = \frac{4}{3}\pi r_u^3 \rho_u n_T n_{p,200} \quad (3.2)$$

where

$$\begin{aligned} M_{f,200} &= \text{mass of fuel in Sangamon200[g]} \\ r_u &= \text{the radius of the UCO kernel inside a TRISO particle[cm]} \\ \rho_u &= \text{the density of UCO in } [\frac{g}{cc}] \\ n_T &= \text{number of TRISO particles in one pebble} \\ n_p &= \text{number of pebbles in Sangamon200} \end{aligned} \quad (3.3)$$

Using the parameters in 3.1, the power density of Sangamon200 and Sangamon20 is 0.11 [kW/g] . With a power capacity of 20 MWth, one can calculate the total mass of UCO in Sangamon20 as

$$M_{f,20} = \frac{P[\text{kW}]}{\rho_p[\frac{\text{kW}}{\text{g}}]} = 181818.18[\text{g}] \quad (3.4)$$

The mass of fuel in a single pebble can be found using the density of UCO and the total volume of UCO kernels in a single pebble, as above. The number of pebbles in the entire reactor, then, is found by dividing the total mass of fuel by the mass of fuel in one pebble, as follows:

$$n_{p,20} = \frac{M_{f,20}}{\frac{4}{3}r_u^3 n_T \rho_u} \quad (3.5)$$

Rounding up - there can only be complete pebbles - we arrive at the number of pebbles in 3.1.

Knowing the number of pebbles is insufficient - the exact dimensions of the active core region are still undefined. To determine the volume of this space, the concept of the packing fraction - the ratio of the volume of objects (the pebbles) to the total volume of their container (the active core) - can be used. The packing of even uniform objects in a 3-dimensional space is a complicated problem, often analyzed in the context of material studies or grain silos [11]. For this reactor, it is assumed the pebble behavior can be described as random loose packing [11] - the pebbles have unsystematically fallen into the core and the core is not shaken. Such packing generally has a packing fraction in the range of 0.56 to 0.60 [11]. Using the definition of the packing fraction, and previously defined terms, the active core volume is

$$V_{c,20} = \frac{n_{p,20} \frac{4}{3} \pi r_p^3}{\phi} \quad (3.6)$$

Using the formula for the volume of a cylinder, one can plot possible sets of $r_{c,20}$ and $h_{c,20}$ that satisfy the volume requirement.

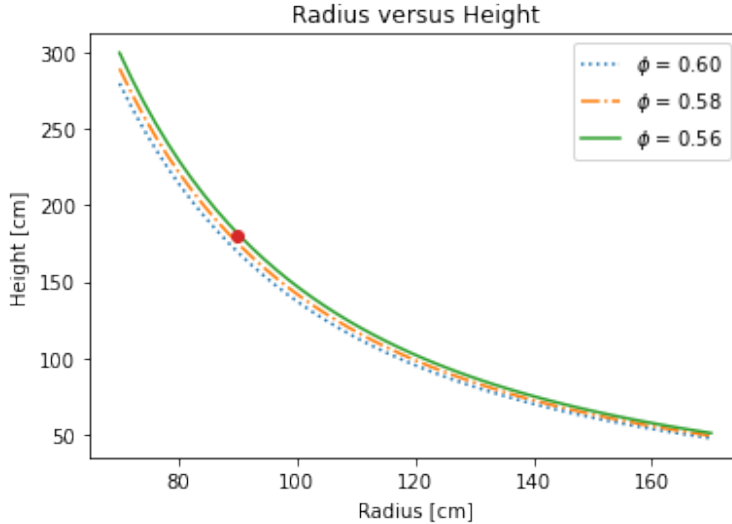


Figure 3.4: Curve of Possible Height and Radii by Packing Fraction

The most critical configurations for a cylinder are either a *square* shape, in which the height is equal to the diameter, or a *flat* shape in which diameter is significantly greater than height. As a flat shape is disadvantageous for a thermal reactor, the former is chosen. The point indicated in 3.4 shows the radius and height selected for Sangamon20 - a radius of 90 cm, and a height of 180 cm.

3.2.2 Graphite Reflector Thickness Determination

The reflector must be sufficiently thick to keep the reactor critical, and protect the pressure vessel. To ensure this, the outward current must be less than or equal to the outward current in Sangamon200 at the outer reflector boundary. The detector layout in Sangamon20 is identical to 3.3.

3.3 Fuel Composition

The number of passes the pebble has theoretically experienced determines its isotopic composition. Seven possible pebble compositions exist, one for each of the six 6-month passes, plus an additional composition for fresh pebbles. The seven pebble compositions are represented equally in number in the core, and they are randomly distributed

throughout the core.

The exact isotopic composition is approximated by running a burnup calculation using Serpent2 for a single pebble in a cube. It uses a reflective boundary condition to simulate the presence of other pebbles or the reflector. The void in the square is filled with helium. While the full-core models homogenize the pebbles, the single-pebble burnup model individually models each TRISO particle. Just as with the location of the pebbles in the full core, the Serpent2 particle dispersal routine generated the TRISO particle locations.

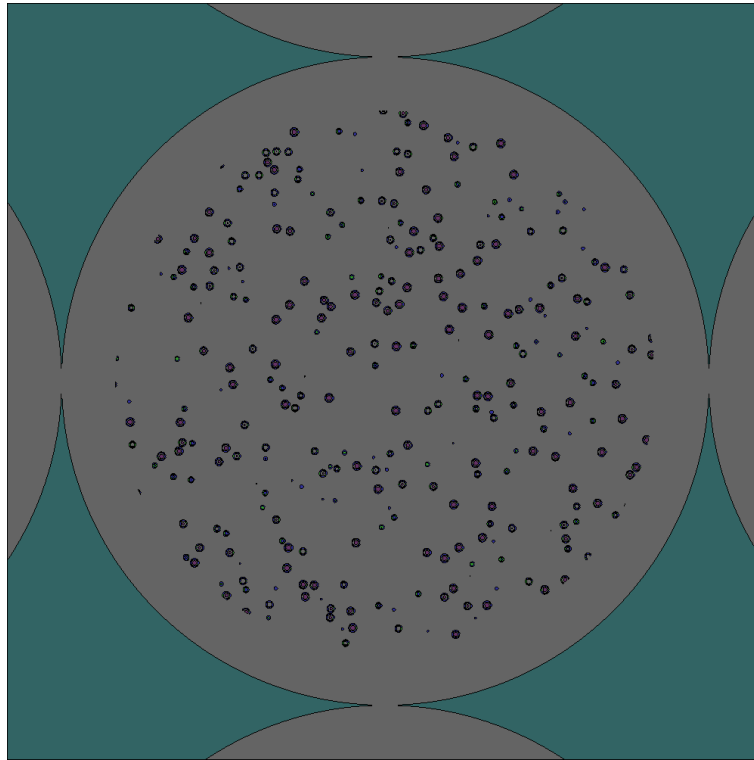


Figure 3.5: Geometry of the Single-Pebble Burnup Calculation: Sangamon20

Once the isotopic compositions are determined, the pebbles are homogenized by volume, to improve performance. The volume of a TRISO particle, and more specifically, a UCO kernel, is assumed constant.

3.4 Reactor Sensitivity to Pebble Locations and Symmetry

As the pebble locations and compositions are determined randomly, it is entirely possible to have bands in the reactor where multiple pebbles of same (or similar) burnup form lines or pockets. In the interest of better characterizing the neutronics of the reactor, a sensitivity analysis tested various pebble composition locations. The *shuffling* test maintained the pebble locations, but changed what composition the individual pebbles were. A second test completely changed the location of the pebbles in the core by randomly dispersing them again. The

third analyzed the effects of utilizing a symmetry simplification, in order to improve computational speed. The core was approximated using a $\frac{1}{6}$ slice. The slice used to simplify changed in each test, shown in 3.6. In each test, all other parameters remain the same.

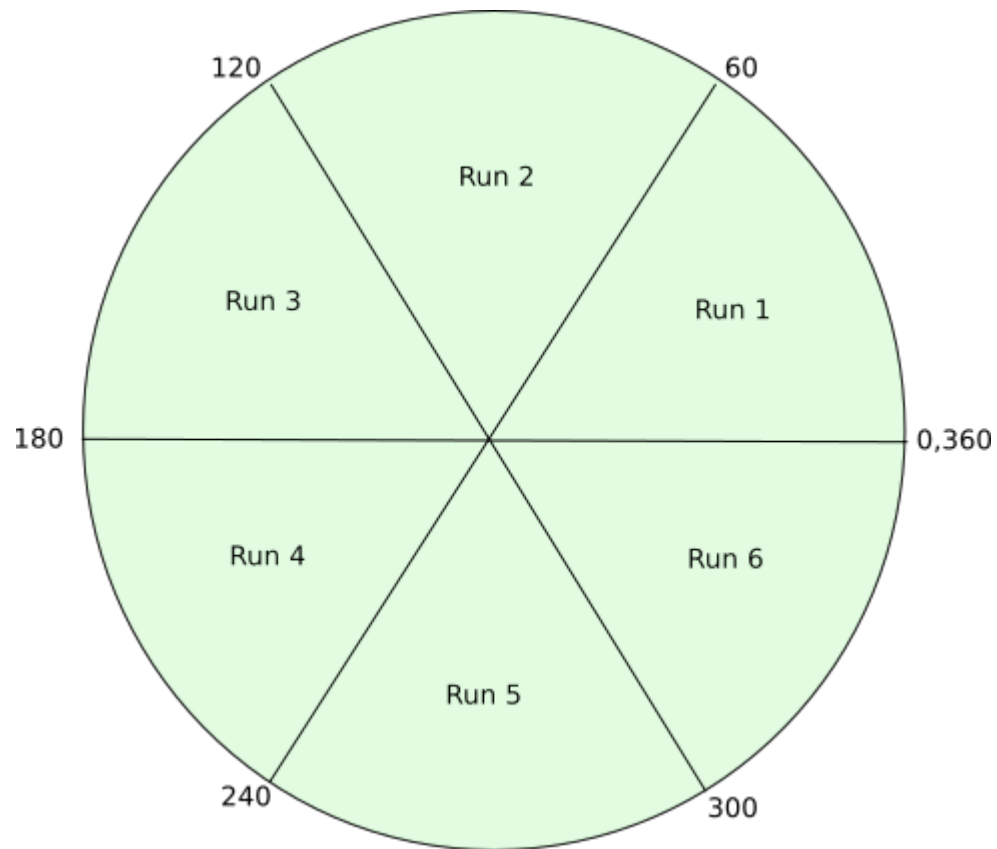


Figure 3.6: Symmetry Test Run Layouts

Chapter 4

Results

*** messages surrounded by three * are notes to the reviewer, if you'd like to ctrl-f for them ***

4.1 Fuel Isotopic Compositions

***Figures in general need to be resized and possibly split into more separate figures than what i'm using right now. if you have any recommendations, they'd be super helpful. Also, I've had trouble overriding latex's figure placement rules, so some of them aren't where I intend them to be. I'm using [h!] in all of them, which *should* place the figure approximately where I place it in the text, and ignore latex's internal figure placement rules. This is not producing the desired effect :(***

The isotopic compositions used in the Sangamon20 full-core models are generated using an infinite cubic lattice of pebbles, which use explicitly modeled TRISO particles. The fuel is exclusively fresh at the first depletion time step, and goes through six burnup cycles, each lasting six months. Figure 4.1 provides the evolution of the fission rate (hot color map) and thermal flux (cold color map) over the 7 stages of burnup. The maximum cutoff for thermal flux is 0.625 eV in these figures. As one might expect, the fission rate decreases over subsequent depletion steps, and thermal flux decreases.

these definitely need to be resized, but I didn't want to take up too much space. Should I try to fit 2 figures side by side, or should I do them one at a time?

The full isotopic inventory tracked in the Sangamon20 reactor models extends far beyond those supplied in 4.2. For a full list, see ***ref zenodo comps*** for the compositions alone, or ***ref phlox zenodo*** for a complete input file and associated output. The isotopes selected for 4.2 are chosen as they are commonly of interest in reactor physics or safety analysis, and any stable isotopes have been omitted from 4.2.

The inventory of uranium is, of course, quite large, rivaled only by the xenon content. All isotopes of uranium steadily increase over time with the exception of U-235, which is lost as it undergoes fission, ending at 0.0647 by atomic fraction in the sixth pass. U-232, while accounting for the smallest fraction of uranium content, also sees the most dramatic increase over time, increasing by two orders of magnitude between its first (9.28E-12) and sixth

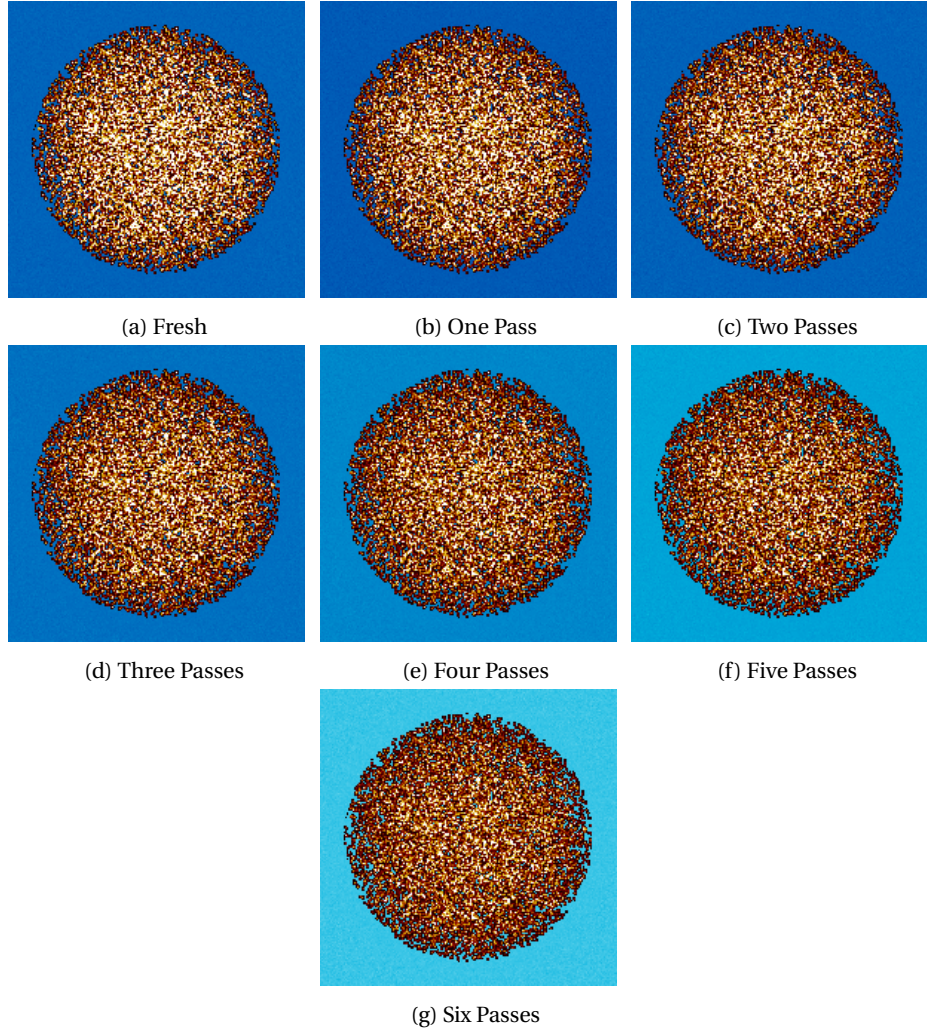


Figure 4.1: Mesh Figures For Single Pebble Burnup

(1.9E-10) cycle. While the atomic fraction doesn't reach an equilibrium, the rate at which it increase each cycle is steady by the third pass, increasing by 4.02E-11, 4.2E-11, and 3.9E-11 from the third to fourth, fourth to fifth, and fifth to sixth pass, respectively. Plutonium content is also fairly high, with Pu-239 peaking at 0.00439. However, unlike many other isotopes which peak in the sixth cycle, Pu-239 crests in the third and fourth passes, only to decrease from 0.00439 in the fourth pass to 0.00380 in the sixth. Pu-238, meanwhile is the least abundant, but does experience the most dramatic increase over time, especially between the first and second passes.

Xe-133 seems to be steady around its initial value of 2.86E-05 atomic fraction, decreasing only to 2.68E-05 by the sixth pass. Xe-135 decreases a bit more dramatically, going from an initial 9.7E-07 after its first six months, to 6.46E-07 after thirty-six months. Xe-136 is both the greatest contributor to xenon content in the fuel, and the only isotope reported in 4.2b to increase, owing to its long half life. Each cycle, Xe-136 content increases by 0.0011, beginning at a concentration of 0.00105 in the first cycle and ending at 0.0066 after the sixth. Isotopes of iodine form

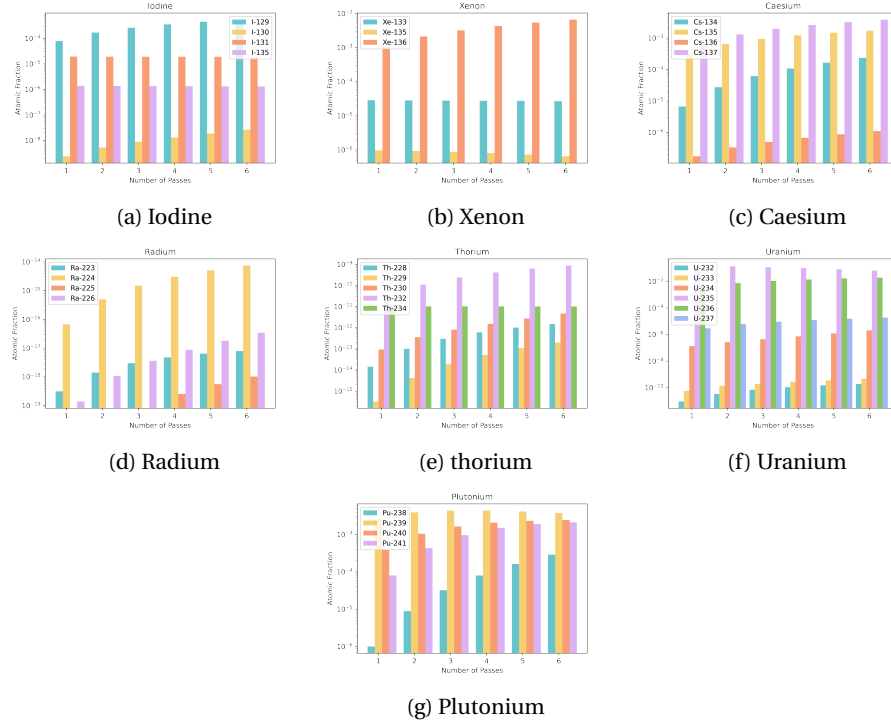


Figure 4.2: Evolution of Certain Isotopic Concentrations in Pebbles over Six Six-Month Passes

a smaller portion of FPs than xenon or caesium, but is still of a relatively high magnitude, and is of concern due to its high mobility in water and uptake in the thyroid. I-129 is the most abundant isotope of iodine reported here, and increases for the entirety of the pebble's life, beginning at 7.38E-05 and peaking at 0.000538 at its discharge burnup. I-130 and I-135 are both relatively stable, most likely due to their short half-lives. I-130 is the least abundant, but increases over time. Caesium has a concentration similar to xenon's, if a bit smaller. Unsurprisingly, Cs-135 and Cs-137, which both have half-lives longer than a pebble's stint in the reactor, are in greatest abundance, and increase over time.

Of the elements reported here, radium and thorium are in lowest abundance. Ra-225 only appears in trace amounts (less than or equal to 9.99E-20) for the first three passes. Ra-224 far outweighs the other reported isotopes of radium, with an atomic fraction of 7.46E-15 after thirty-six months - two orders of magnitude higher than all other isotopes of radium combined at this depletion step. Thorium has the second-least abundant atomic fractions, with fertile Th-232 being the most abundant, at 8.8E-10 in the sixth pass.

4.2 Full-Core Control Model

Figure 4.4 shows a cross section of the core geometry at the origin in the xy and xz planes (a and c, respectively) and provides a mesh of the fission rate and thermal flux in the xy and xz planes (b and d, respectively). Both of these are

integrated to produce a 2D image.



Figure 4.3: Legend for Geometry Figures

Figure 4.3 is accurate for all cross sections of reactor geometry. In homogenized models, the shades of green represent the material blend forming the center of the pebble, at a given burnup. For heterogenized models, these same shades represent the TRISO particle kernel at a particular burnup.

The mesh in 4.4b shows bands of concentric rings around the outer edges of the active core. These bands would suggest that the outermost regions of the core are regions of high fission activity, relative to the center, which is at odds with what most would expect from the neutronics behavior in a cylindrical reactor. Certainly, the pebbles are physically forming rings at the outer edges, and their placement becomes more haphazard toward the center. However, the author asserts that the high intensities seen in this outer region in the mesh figures are not indicative of a total flux profile showing the same. Remember that this image is generated by integrating over the z direction to produce a 2D plot of the xy plane. For a cylinder, the distance in z each point integrates over is the same - the height of the reactor. However, points at the outermost regions are integrating in a volume that is composed more of pebbles - and therefore fissile material - than the center, where there is more space filled with coolant.

In figure 4.4d we can see a similar banding effect on the top and bottom edge of the core region, but not on the sides. There are no hotspots on the edges because 4.4d is in the xz plane, and integrates over y. However, for a cylinder, the distance integrated over is not the same at all points. At the centerline, the distance is simply the diameter. However, as you move towards the edge, the distance integrated over approaches zero.

***I know that there should be continuity at 0 between the axial and radial flux profiles, and there currently is a difference of 3 orders of magnitude. I believe this is because of differing bin sizes between the detector that tracked the axial fluxes, and the detector that tracked the fluxes at the xy plane. Basically, in the axial detector, each bin had a defined length in z, 0.1 cm or what-have-you. However, these bins had no x or y limitations, and covered all x and y at that point (the bins are shaped like a stack of pancakes or such). For the radial detector, I had to create the detector bins such that they formed a uniform grid over the xy plane, centered on the origin (which is the physical center of the reactor). These bins were finite in x and y, but not in the z direction, so they covered all z that fell within

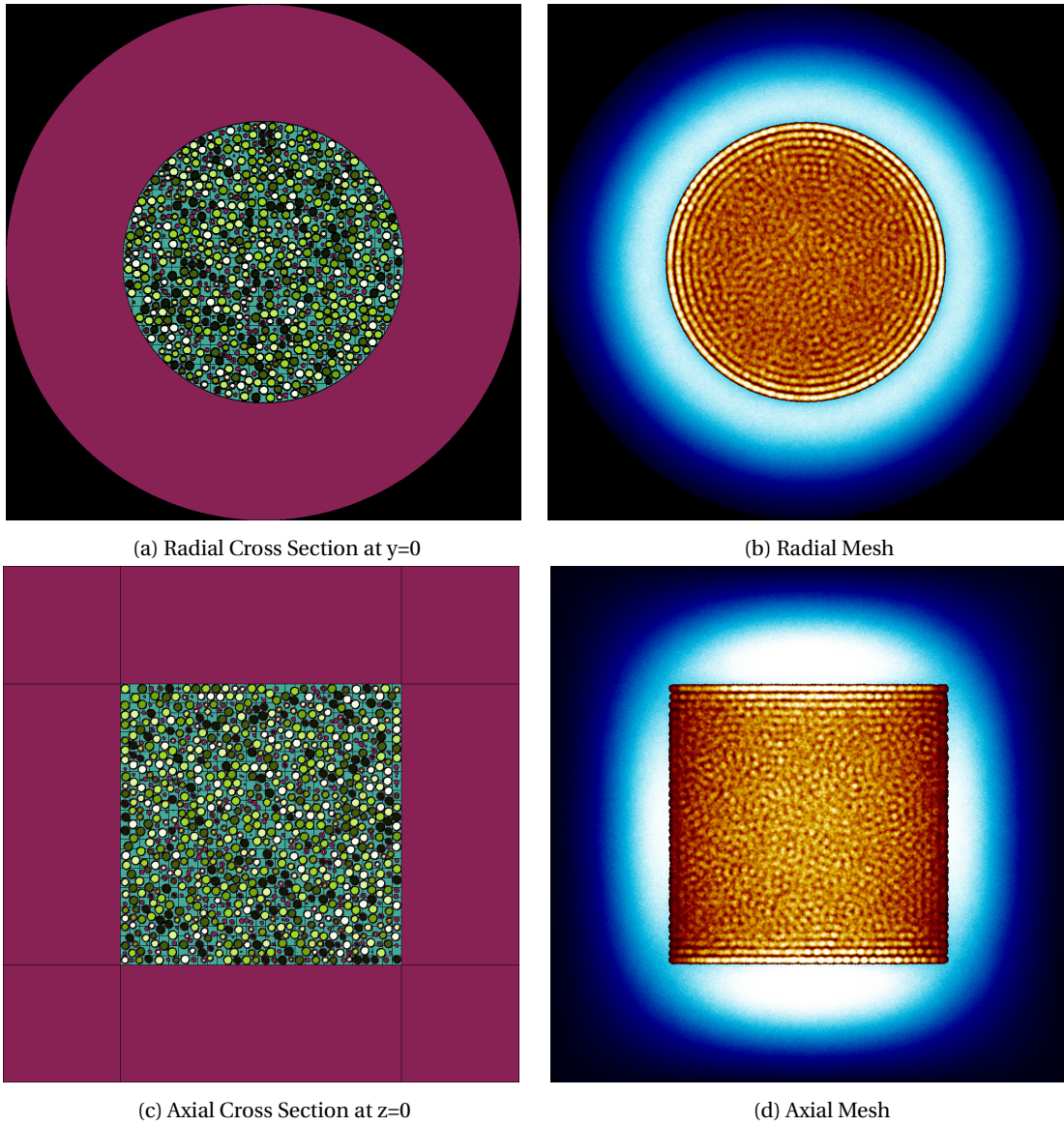


Figure 4.4: Full Core

the limits of the bin (these bins are like a long rectangular prism). While this uniform grid prevents the radial flux profile from warping, which is what happens if you attempt to make a detector along only one axis (the bins end up being unequal sizes), the fact that the axial detector bins differ from the radial detector bins means they don't match each other.

tl;dr: should I divide the neutron flux by bin volume so the axial and radial profiles match in magnitude (hopefully)***

Figures 4.5 and 4.6 provide the fast and thermal flux profiles in Sangamon20. The former are the radial fluxes, along the x-axis, and the latter are the axial center line ***can I just say center line?*** profiles. Both axially and

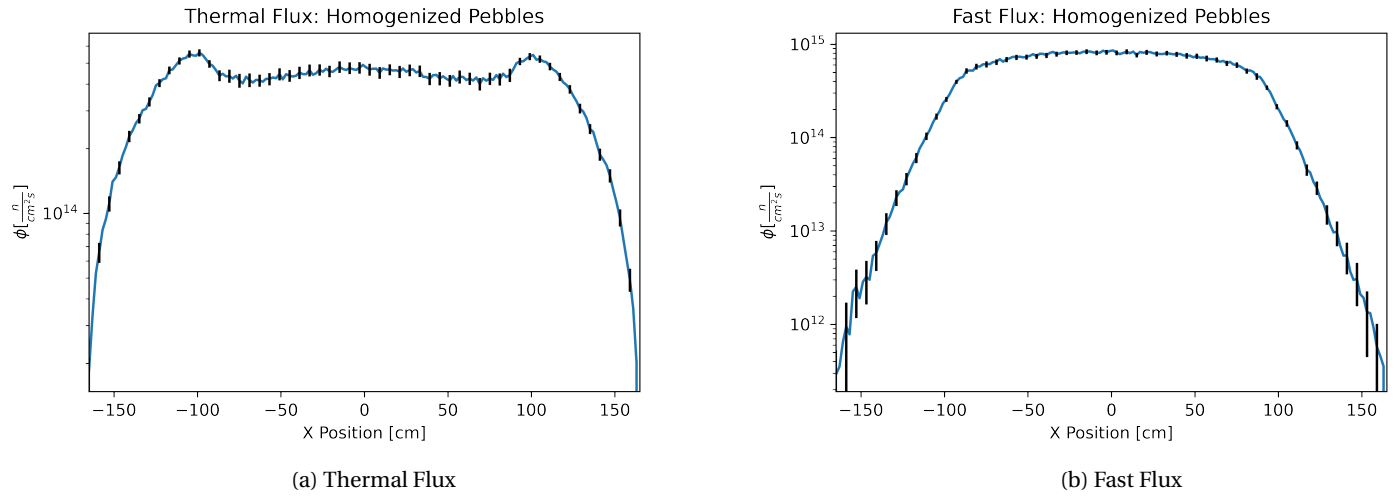


Figure 4.5: Radial Thermal and Fast Flux Profiles

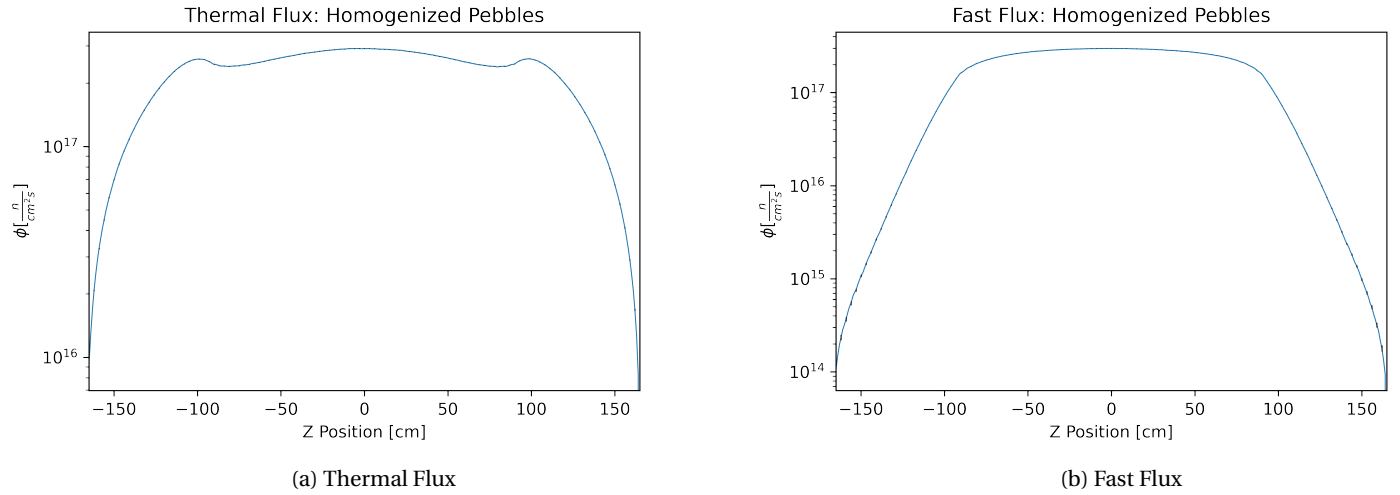


Figure 4.6: Axial Thermal and Fast Flux Profiles

radially, the thermal flux sees a 'bump', which peaks approximately 10 cm into the reflector, at 100 cm. These are the highest peaks in the thermal flux, with the second highest thermal flux being at the center line. For the fast flux profile, we see a flattened peak in the active core (-90.0 cm to 90 cm) and 10 cm into the reflector. Fast flux rapidly decreases in the reflector, as fast neutrons down scatter in the graphite.

Both 4.5 and 4.6 show that the radial banding seen in the fission rate mesh profiles, which appear to be of a very high intensity, are not actually where the true peaks in the flux profiles are located.

***okay, these mesh figures in particular I A) have a lot of trouble getting to a good size and B) kinda want to make big to see detail (especially since I discuss some of the finer details in the image). Maybe I could show a smaller version here, and then add a larger version in the appendix, where it doesn't matter if my mesh plot takes up

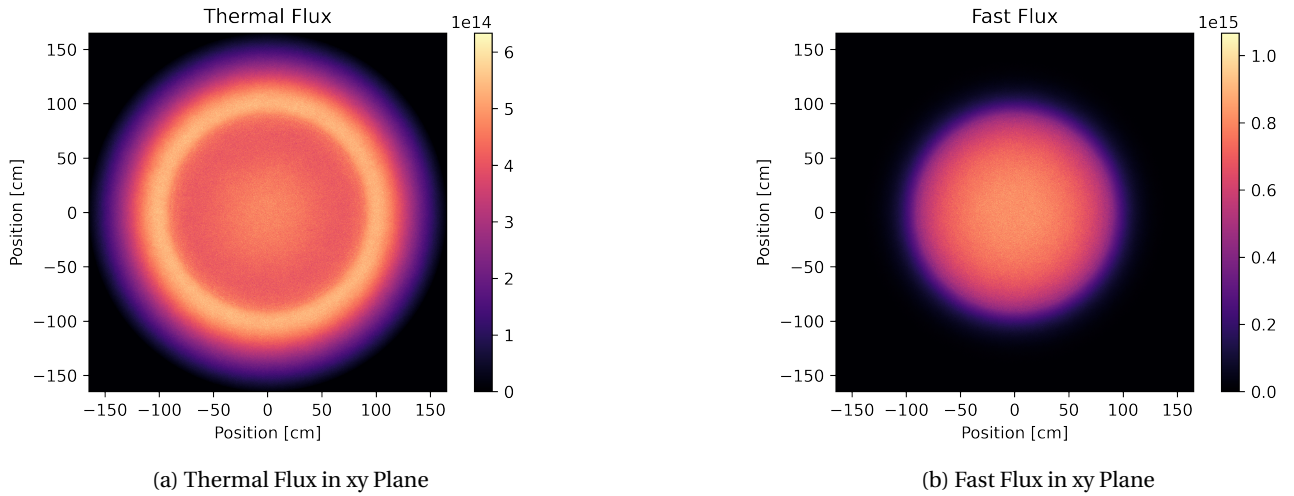


Figure 4.7: Thermal and Fast Flux Profiles

its own page. ***

Figure 4.7 provides the total flux over the xy plane at $z = 0$. A slight banding pattern on the active core's edge can be seen, but not with the same intensity of the fission rate banding. Once again, figure 4.7 shows that while the banding morphology may be present in the flux profile (and do cause a slight increase relative to the region immediately surrounding it) it does not cause large concentric spikes in the flux profiles.

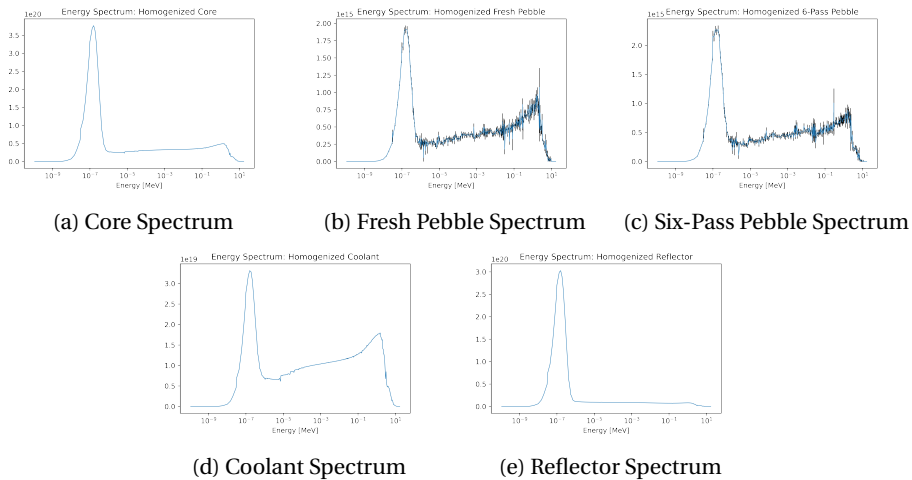


Figure 4.8: Lethargy Adjusted Neutron Flux Energy Spectra

***these bad boys need to be bigger for sure Also, while "homogenized pebbles" would be accurate, "homogenized coolant" and "homogenized reflector" make it sound like I did something to those materials, but I didn't. I think at one point I used "Coolant of a Core Using Heterogenized Pebbles" but that's a bit long. ***

Above, the energy spectra in the reflector, coolant, overall core, and a randomly selected fresh and 6th-pass

pebble are provided. The results are per unit lethargy and use the Tripoli 315-group energy structure.

The thermal peak of the whole-core and reflector both occur around 10E-07 MeV, which is also the energy of neutrons most-responsible for fission in this model. The thermalization of neutrons in the reflector dominates the spectrum in 4.8a, indicated by the high magnitude of the thermal peak in the reflector and core and their similar shape.

The spectra for a randomly selected fresh and 6 pass pebble are subject to the highest uncertainty of all the provided spectra in 4.13, as a single pebble is a relatively small bin. However, when coupled with the coolant spectra, 4.8d, they provide a clearer look at the flux energy spectrum in the active core region. We can see that, while the thermal energy of the fresh and six-pass pebbles are similar in shape and magnitude, there is considerable difference in the higher energy range, due to the buildup of fission products and the decrease in U-235 concentration.

4.3 Effect of Homogenizing

The results above all use the assumption of a pebble that has the TRISO particles homogenized and blended with the rest of the pebble matrix in the region containing fuel. However, as reported in [47], homogenization can cause under-predictions of k-eff as large as 5-6%. And so, an otherwise identical model with explicitly modeled TRISO particles (the fuel kernel and all four protective layers are explicitly modeled) is used to investigate the effect of homogenization. As a reminder, the isotopic compositions are pulled from a burnup simulation using an infinite lattice of pebbles with explicitly modeled TRISOs. As such, the isotopic compositions between the homogenized and heterogenized models are identical.

In agreement with [47], the heterogenized model reported a k-eff of 1.087 +/- 0.00032, compared to the homogenized model's 1.041 +/- 0.00054, a difference of 4.23%.

Overall, the mesh result for the fission rate is much the same - the banding patterns are still present, if slightly less defined. While 4.9 best serves as a qualitative visualization aid, figures 4.10, 4.11, and 4.12 support this in a more quantitative manner.

Compared to the homogenized model, the heterogenized Sangamon20 core reports a slightly lower neutron current at the outer edge of the reflector, at 5.718E+11 +/- 1.735E-09, an absolute difference of approximately 2.0E+09. The heterogenized model otherwise shows a similar flux profile to the homogenized model, and experiences a similar level of uncertainty in the outer edges of the reflector for the fast flux profiles, likely due to the significant thermalization of neutrons by that point in the reflector.

Compared to Figure *** ref homo xy plane mesh **, the edge pebble bands are much less distinct. This is because the homogenized pebbles have the fissile material spread over the entirety of the 2.5 cm radius fueled center. The

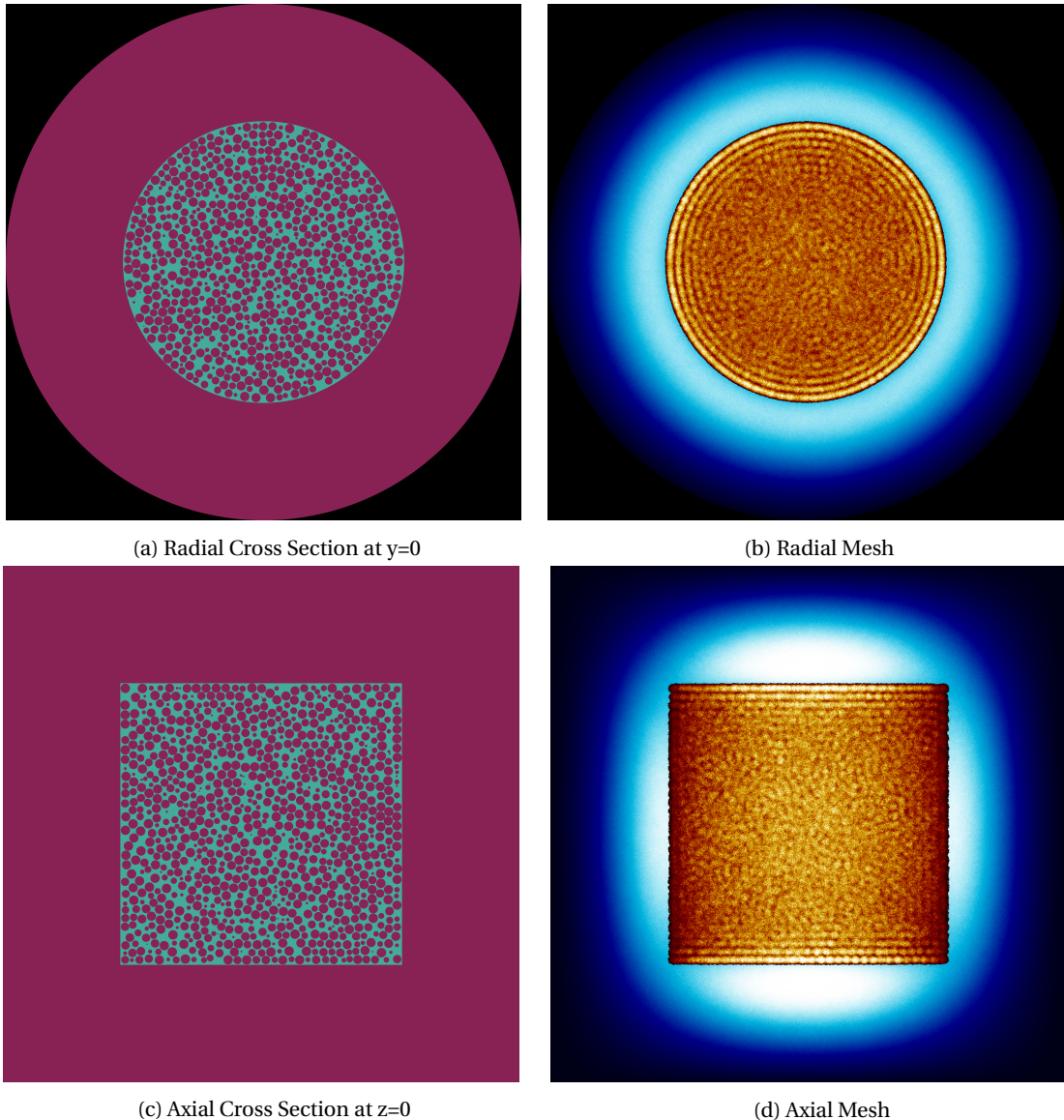
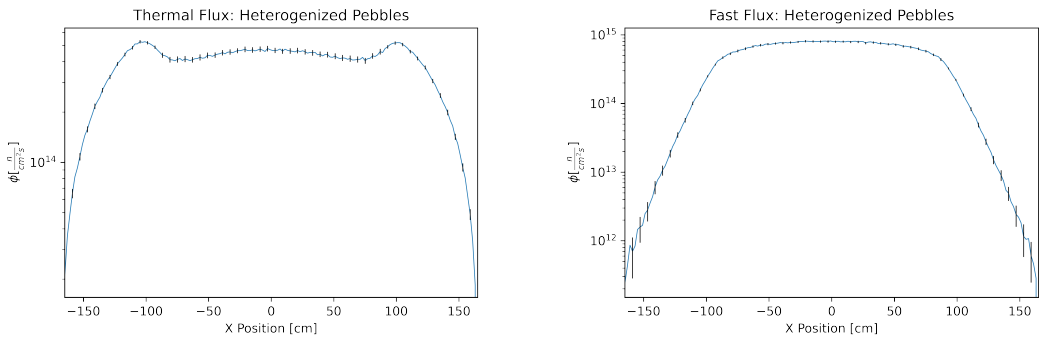


Figure 4.9: Full Core Using Heterogenized Pebbles

heterogenized pebbles, meanwhile, may have the same number of fissile atoms, but the regions capable of fission are concentrated to the TRISO kernel. The rest of the pebble consists of its graphite matrix.

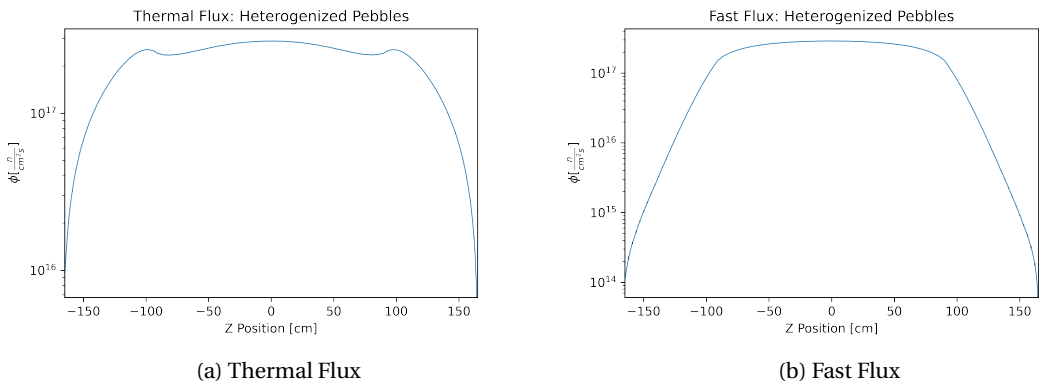
The heterogenized spectra, much like the flux profiles, are of a very similar morphology. In order to better examine the differences between the homogenized and heterogenized models, simple relative difference was calculated and plotted for all spectra, and the radial fast and thermal profiles. The relative difference was calculated according to the following:



(a) Thermal Flux

(b) Fast Flux

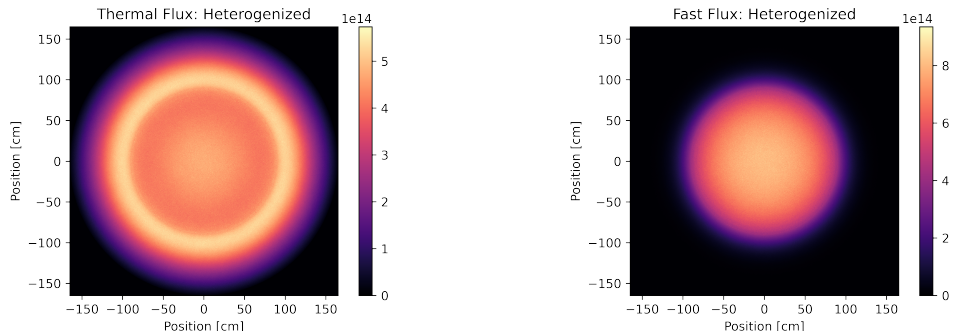
Figure 4.10: Radial Thermal and Fast Flux Profiles: Heterogenized Pebbles



(a) Thermal Flux

(b) Fast Flux

Figure 4.11: Axial Thermal and Fast Flux Profiles: Heterogenized Pebbles



(a) Thermal Flux in xy Plane: Heterogenized Pebbles

(b) Fast Flux in xy Plane: Heterogenized Pebbles

Figure 4.12: Thermal and Fast Flux Profiles

$$\Delta i = \frac{i_{hom} - i_{het}}{i_{het}} \quad (4.1)$$

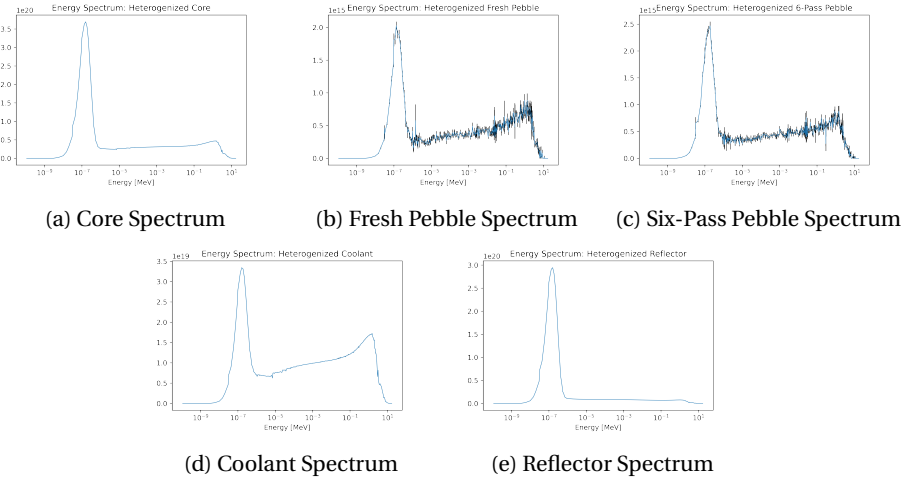


Figure 4.13: Lethargy Adjusted Neutron Flux Energy Spectra: Core Using Heterogenized Pebbles

where

Δi = relative difference for parameter i between homogenized and heterogenized model

i_{hom} = homogenized parameter i

i_{het} = heterogenized parameter i

(4.2)

And error was calculated using simple error propagation rules.

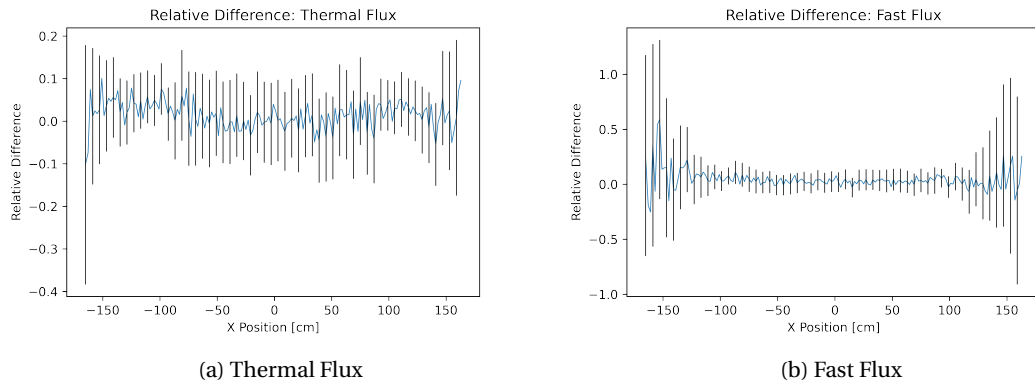


Figure 4.14: Relative Difference in Radial Thermal and Fast Flux Profiles Between Cores Using Homogenized and Heterogenized Pebbles

For both the thermal and flux profiles, the higher error at the edges of the flux profile is exacerbated. Overall, 4.14a and 4.14b suggest that the homogenized model is slightly over-predicting the magnitude of the flux, however,

given the size of the error, these differences cannot be said to exist with certainty.

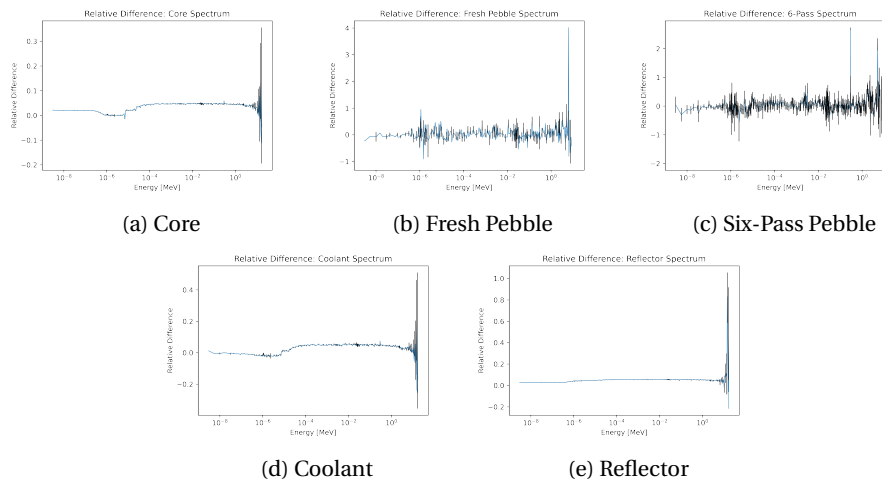


Figure 4.15: Relative Difference in Lethargy Adjusted Neutron Flux Energy Spectra Between Cores using Homogenized and Heterogenized Pebbles

Overall, the homogenized model is over-predicting the thermal peak compared to the heterogenized model in the core spectra by approximately 5%. At approximately 10E-06 MeV, just after the thermal peak, the two spectra have a brief moment of agreement before diverging again, this time with a slightly larger disagreement. Unlike 4.14, the relative differences seen in 4.15 are not accounted for by error alone, with the exception of the highest neutron energy ranges. ***should I leave these, and include an image that gives a close up of the areas of interest, so the huge error at the tail end doesn't keep the reader from seeing detail?***

The coolant spectra differed from each other after the thermal peak in a magnitude and shape matching the differences in core spectra. Unlike the core, however, the coolant has much closer agreement at lower energy levels, including at the thermal peak. The reflector shows, if any, a very slight over estimation on the part of the homogeneous spectra, which is consistent for all but the highest energy levels.

It is in the pebble spectra that we see the most dramatic disagreement. Around the thermal peak, in both 4.15b and 4.15c, there is a spike in the relative difference, though the error is still substantial in this region compared to the peaks in the relative difference. Between the thermal peak and 5E-02, the differences are minimal and can be accounted for by noise or error. Between 10E-02 and 10E-01, however, there is a slight blip, which may be indicative of a fission product with a resonance around this region **I don't think I said that quite right*** being affected by having graphite surrounding it more directly.

The most dramatic peaks occur in the six-pass pebble at 0.2995 MeV, which indicates that the homogenized reactor is over-predicting the lethargy-adjusted neutron flux at this energy level. To be precise, the homogenized pebble model is over-predicting in this region by a factor of 2.69. In both the fresh and six-pass pebble spectra, there

is a peak at *****. One possibility is that the U-235 in the pebble is more likely to undergo fission in a homogenized pebble, which disperses the U-235 atoms in what is almost pure graphite, compared to the heterogenized pebbles, which, while some U-235 atoms may be directly next to graphite, are most like near other U-235 atoms. That the peak in the fresh pebble is so much higher - a factor of 4 - compared to the six-pass pebble - a factor of 2 - also is another sign.

4.4 Sensitivity Tests

Beyond a comparison of homogenized versus heterogenized pebbles, the effects of two other model changes were investigated. The first looks at the effects of assuming a $\frac{1}{6}$ core symmetry, the other is a simplified test of changing pebble locations - changing the fuel composition in each pebble, rather than entirely re-generating pebble locations using the dispersal routine. All tests compare models using the homogenized pebble assumption as a base.

4.4.1 Effects of Symmetry Assumption

Overall, the effects of using a $\frac{1}{6}$ core symmetry were minimal.

Run	k_{eff}	$J^+ [\frac{n}{cm^2s}]$	$J^+ \% \Delta$ Sangamon20
Run 1	1.03990 ± 0.00055	$5.921e+11 \pm 2.900e-09$	0.637%
Run 2	1.03979 ± 0.00050	$5.884e+11 \pm 2.781e-09$	0.000%
Run 3	1.04150 ± 0.00054	$5.908e+11 \pm 2.485e-09$	0.402%
Run 4	1.03927 ± 0.00057	$5.910e+11 \pm 2.900e-09$	0.436%
Run 5	1.04154 ± 0.00054	$5.884e+11 \pm 2.978e-09$	0.000%
Run 6	1.04047 ± 0.00050	$5.888e+11 \pm 2.840e-09$	0.067%

Table 4.1: Run Summary

Below, 4.16 provides cross-sections of the geometry, and fission rate/thermal flux meshes for the one-sixth core symmetry test. The fission rate mesh naturally exhibits a repeating pattern with six-points of symmetry, and still shows the banding patterns on the outer edges.

*** alright, I tried to convey my observation as best I could, but I have a suspicion it isn't nearly as clear on paper as it is in my head. Any suggestions are welcome, and if it seems like it would be better to leave this section out, I can*** One point of interest, however, is the degree to which the region from 0 to 60 degrees matches the same region in the control model. Figure 4.17 was generated by subtracting the radial meshes for the control and first symmetry test.

Unsurprisingly, in the areas outside the 0 to 60 degree slice, the two fission rate meshes disagree quite a bit. However, within this region, the two meshes are almost identical, pixel for pixel. While this might be expected towards the center of this region, the perfect match towards the edges of it are less so. As a reminder, the symmetry

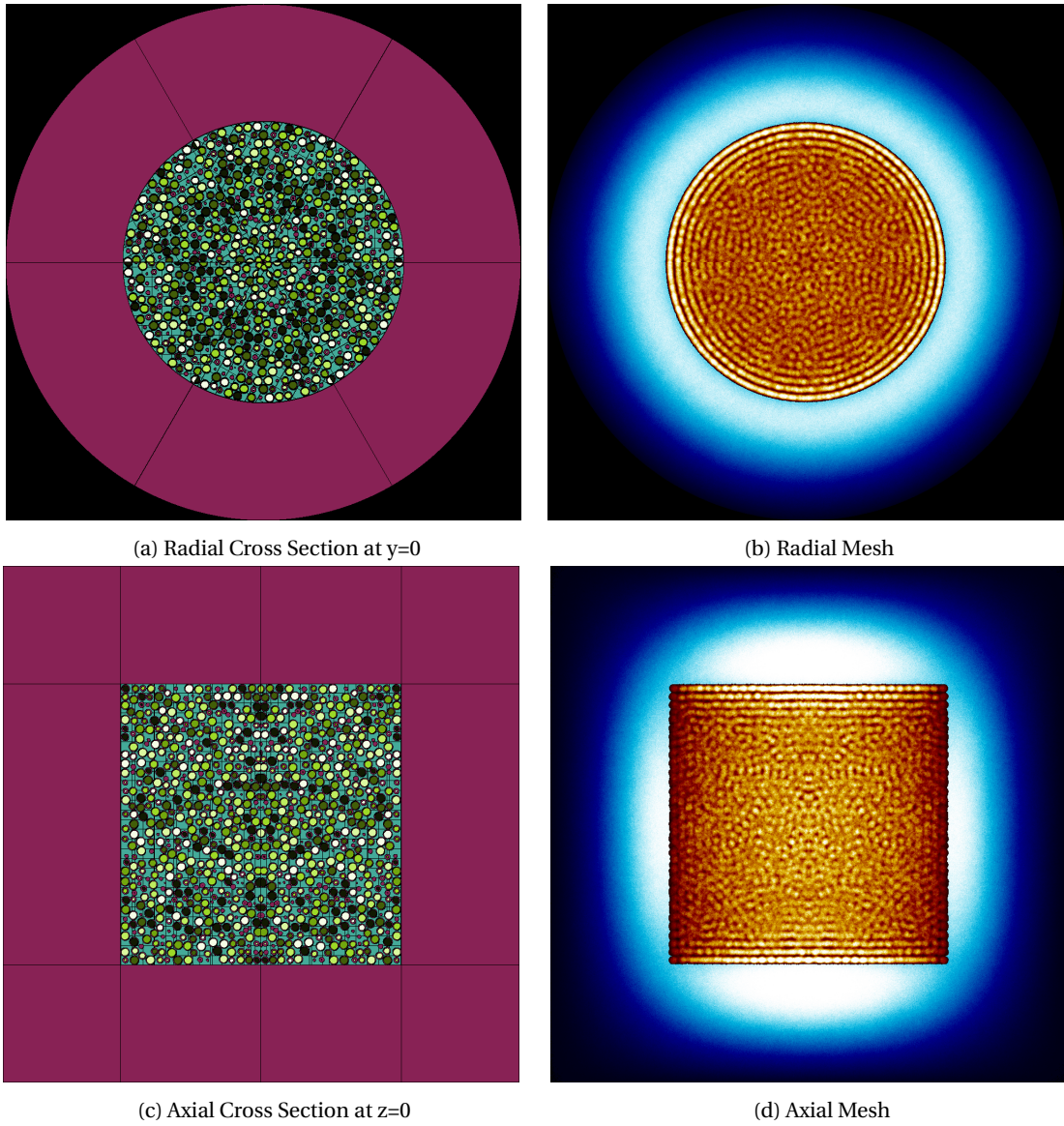


Figure 4.16: Sensitivity Analysis: $0^\circ - 60^\circ$

tests all use a one-sixth symmetry, and a periodic boundary condition, i.e., when a neutron leaves the slice on one side, it re-enters the slice on the other. In effect, the edges of the $0-60$ slice in the symmetry test are seeing entirely different materials, compared to the control. That there is not a gradient of difference at the edges in 4.17, but rather a hard line, may suggest that, with proper mixing, nearest-neighbor pebbles do not have a very strong effect. However, it is important to note that Sangamon20 uses only fuel pebbles, and this observation may not hold true in a reactor design using, for example, adsorber pebbles.

I think I should put these in the appendix and directly reference them here - there just isn't enough "new" to say for each of the figures that warrants them all being in the main body, I think?

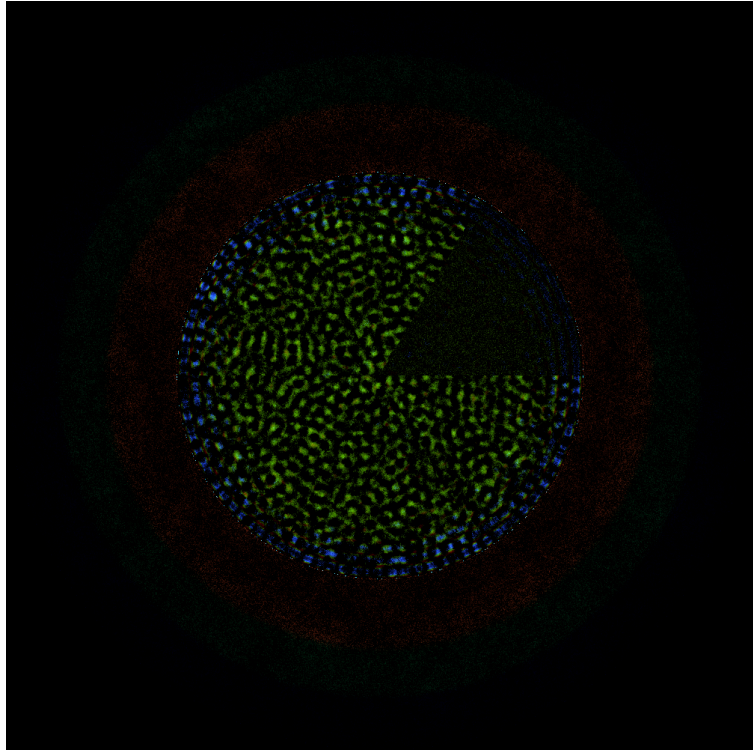


Figure 4.17: An Image Generated by Subtracting 4.16b from 4.17.

- as above, but the 120-180 degree slice
- as above, but the 180-140 degree slice
- as above, but the 240-300 degree slice
- as above, but the 300-360 degree slice

4.4.2 Effects of Pebble Shuffling

The final test on the effects of changes to core modeling is another test of consistency between similar HTGR models with a different pebble configurations. Rather than re-generate the pebble locations several times, the 'shuffling' test simply reassigned each pebble with a different fuel composition. For example, the pebbles that were once fresh are now first-pass, the first pass pebbles are now second-pass, and so on. This shuffling was done several times, and the results of this test are in 4.2.

Overall, much like the symmetry test, re-mixing the pebbles had little effect on overall results. Likely, provided the pebbles are sufficiently mixed, and there are not 'pockets' of like pebbles, models that are otherwise identical should provide similar results.

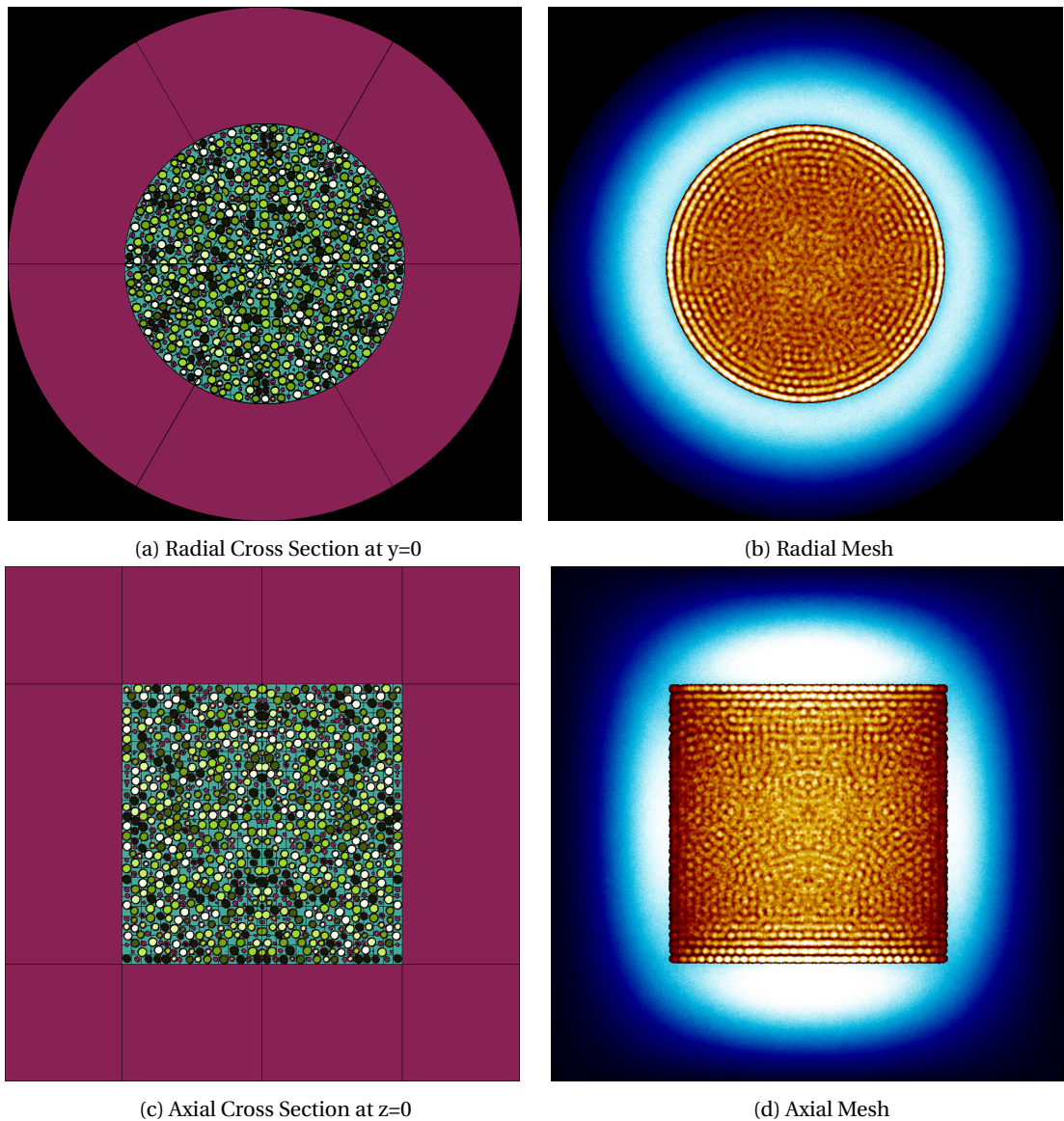
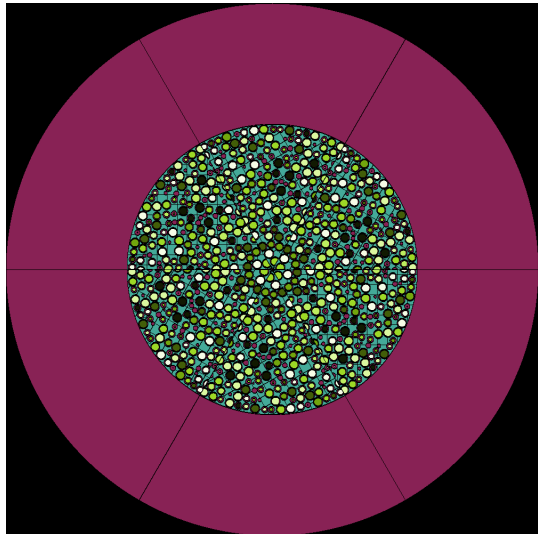


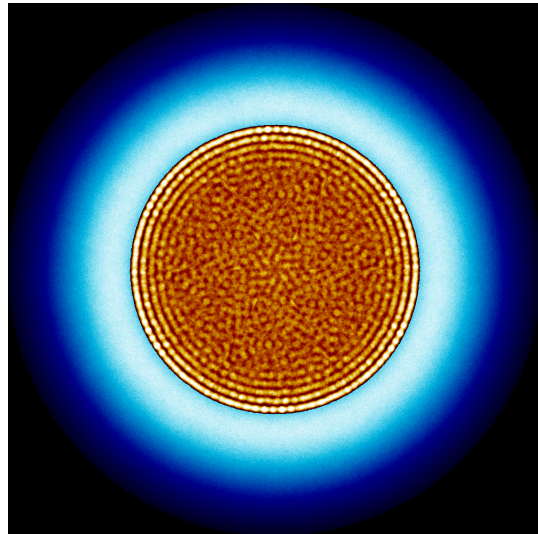
Figure 4.18: Sensitivity Analysis: $60^\circ - 120^\circ$

Run	k_{eff}	$J^+ [\frac{n}{cm^2 s}]$	$J^+ \% \Delta$ Sangamon20 Control
Run 1	1.03990 ± 0.00055	$5.921e+11 \pm 2.900e-09$	0.637%
Run 2	1.04067 ± 0.00050	$5.908e+11 \pm 3.057e-09$	0.402%
Run 3	1.04133 ± 0.00055	$5.888e+11 \pm 2.584e-09$	0.067%
Run 4	1.04206 ± 0.00058	$5.906e+11 \pm 2.840e-09$	0.369%
Run 5	1.03850 ± 0.00060	$5.929e+11 \pm 2.742e-09$	0.771%
Run 6	1.03874 ± 0.00052	$5.939e+11 \pm 2.604e-09$	0.939%
Run 6	1.03746 ± 0.00058	$5.949e+11 \pm 2.623e-09$	1.106%

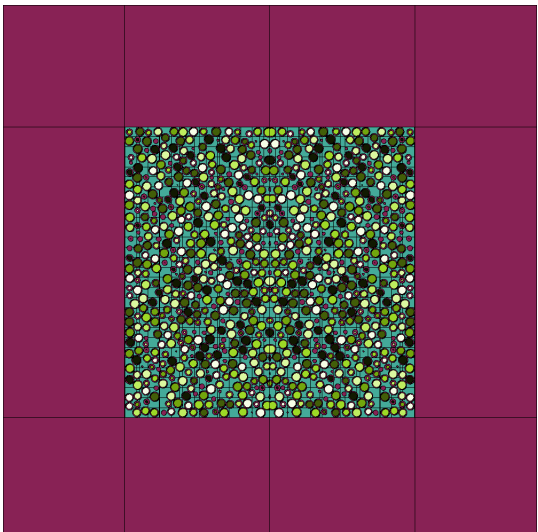
Table 4.2: Run Summary



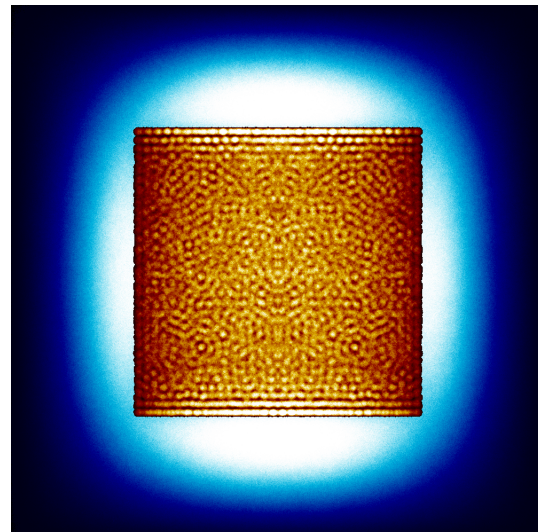
(a) Radial Cross Section at $y=0$



(b) Radial Mesh

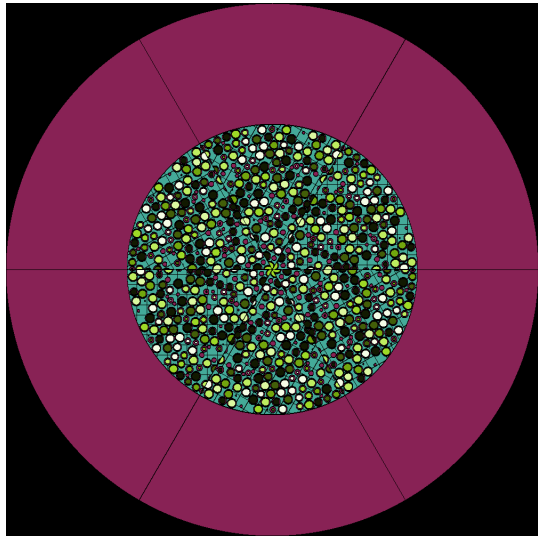


(c) Axial Cross Section at $z=0$

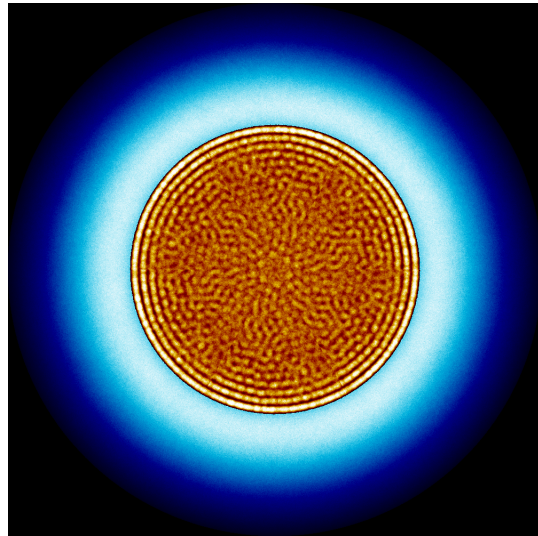


(d) Axial Mesh

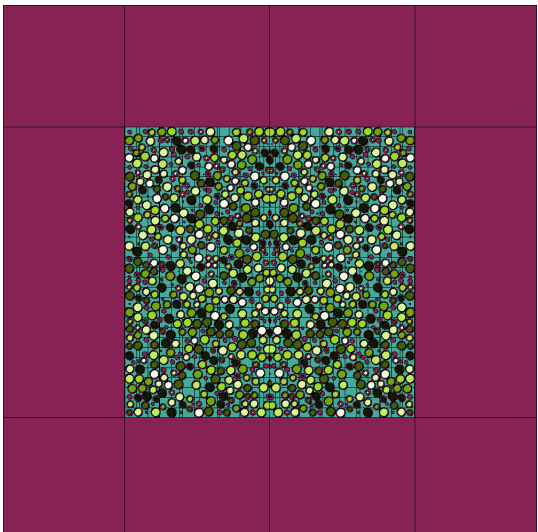
Figure 4.19: Sensitivity Analysis: $120^\circ - 180^\circ$



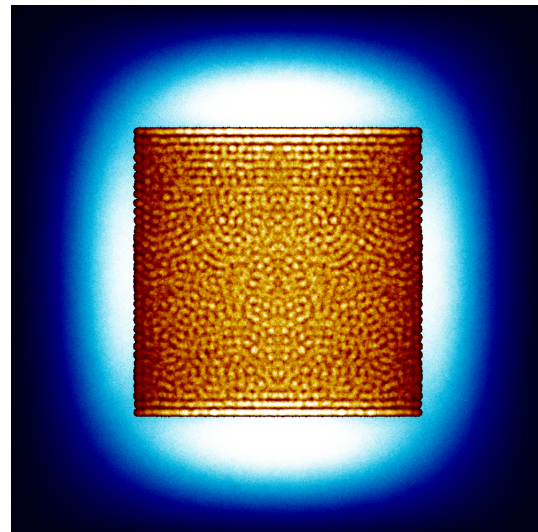
(a) Radial Cross Section at $y=0$



(b) Radial Mesh

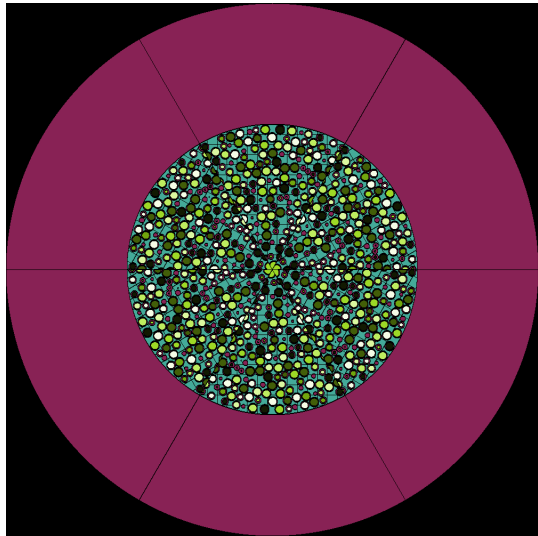


(c) Axial Cross Section at $z=0$

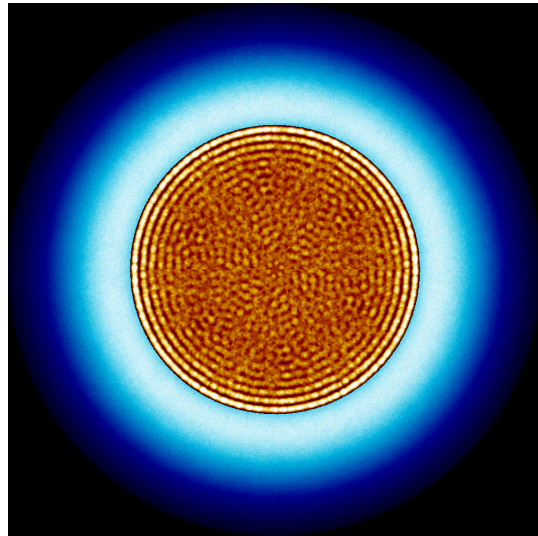


(d) Axial Mesh

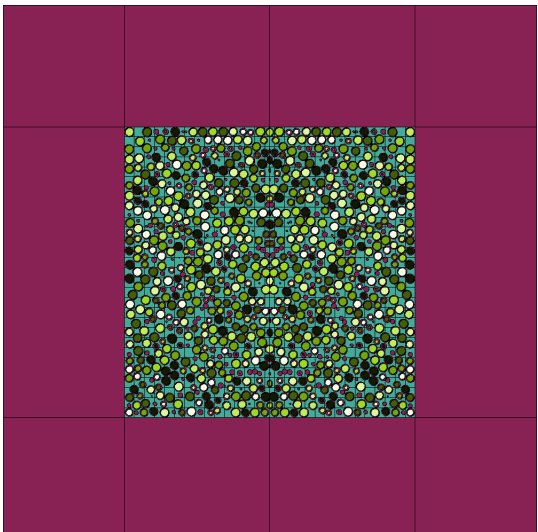
Figure 4.20: Sensitivity Analysis: $180^\circ - 240^\circ$



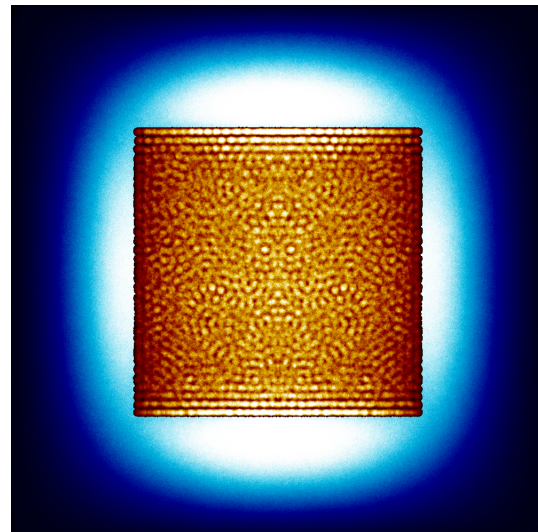
(a) Radial Cross Section at $y=0$



(b) Radial Mesh

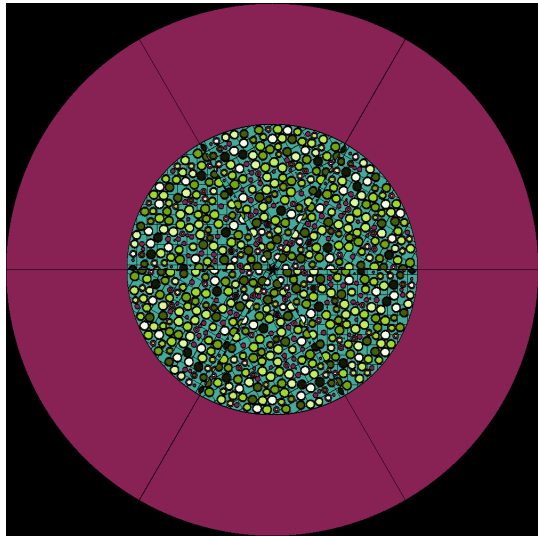


(c) Axial Cross Section at $z=0$

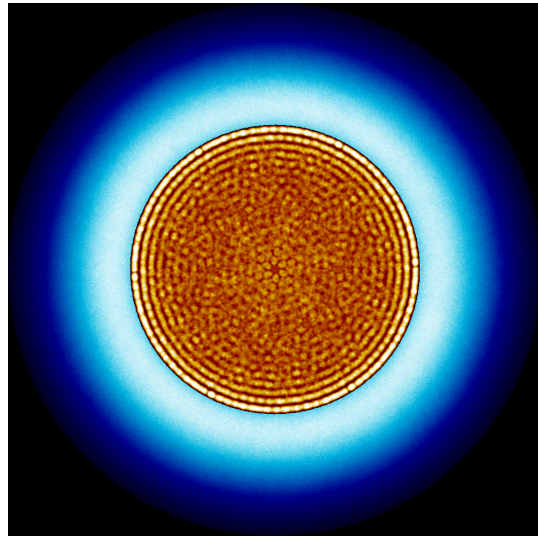


(d) Axial Mesh

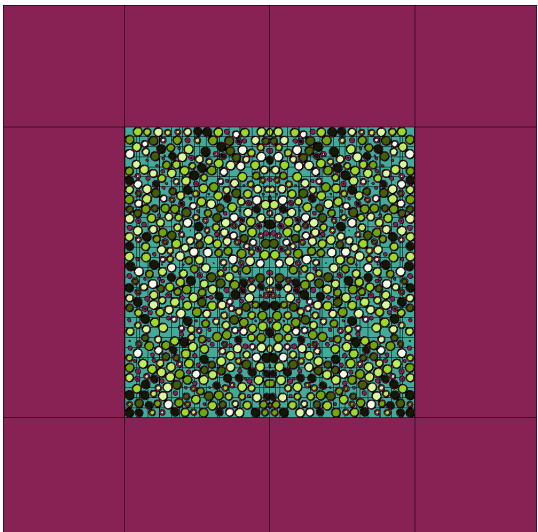
Figure 4.21: Sensitivity Analysis: $240^\circ - 300^\circ$



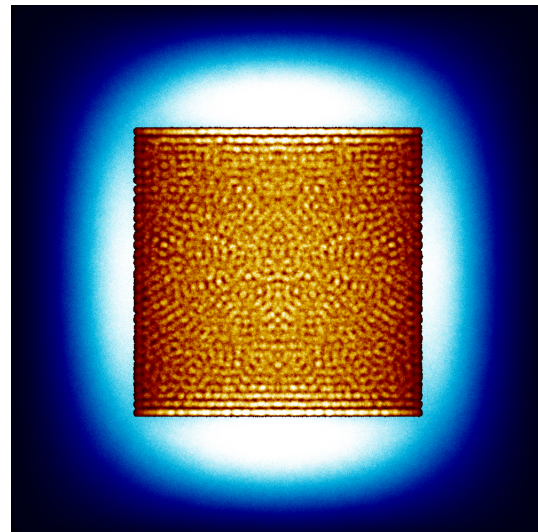
(a) Radial Cross Section at $y=0$



(b) Radial Mesh



(c) Axial Cross Section at $z=0$



(d) Axial Mesh

Figure 4.22: Sensitivity Analysis: $300^\circ - 360^\circ$

Chapter 5

Conclusion

conclusion

Appendix

Appendix.

References

- [1] M. T. Simnad, "The early history of high-temperature helium gas-cooled nuclear power reactors," vol. 16, no. 1, pp. 25–32. [Online]. Available: <https://www.sciencedirect.com/science/article/pii/036054429190084Y>
- [2] J. M. Beck and L. F. Pincock, "High temperature gas-cooled reactors lessons learned applicable to the next generation nuclear plant," p. 78.
- [3] "Results of experiments at the AVR reactor," vol. 121, no. 2, pp. 143–153, publisher: North-Holland. [Online]. Available: <https://www.sciencedirect.com.proxy2.library.illinois.edu/science/article/pii/002954939090099J>
- [4] Serpent - a monte carlo reactor physics burnup calculation code. [Online]. Available: <http://montecarlo.vtt.fi/>
- [5] P. J. Venter, M. N. Mitchell, and F. Fortier, "PBMR REACTOR DESIGN AND DEVELOPMENT," p. 15.
- [6] Areva modular reactor selected for NGNP development - world nuclear news. [Online]. Available: https://www.world-nuclear-news.org/NN-Areva_modular_reactor_selected_for_NGNP_development-1502124.html
- [7] INL. Basis for NGNP reactor design down-selection. [Online]. Available: <https://inldigitallibrary.inl.gov/sites/sti/sti/5223031.pdf>
- [8] B. Harlan, "X-energy xe-100 reactor initial NRC meeting," xe-100 Reactor initial NRC meeting. [Online]. Available: <https://adamswebsearch2.nrc.gov/webSearch2/main.jsp?AccessionNumber=ML18253A109>
- [9] N. Agnihotri and E. Mulder. An intrinsically safe generation IV reactor. [Online]. Available: <http://digitaleditions.nuclearplantjournal.com/SO17/24/>
- [10] J. Leppänen. Serpent – a continuous-energy monte CarloReactor physics burnup calculation code. [Online]. Available: http://montecarlo.vtt.fi/download/Serpent_manual.pdf
- [11] S. S. Tulluri, "Analysis of random packing of uniform spheres using the monte carlo simulation method," p. 107.
- [12] A. T. Cisneros, "Pebble bed reactors design optimization methods and their application to the pebble bed fluoride salt cooled high temperature reactor (PB-FHR)." [Online]. Available: <http://gradworks.umi.com/36/16/3616613.html>
- [13] Amir Afzali, "High temperature, gas-cooled pebble bed reactor licensing modernization project demonstration," u.S. Department of Energy (DOE) Office of Nuclear Energy Under DOE Idaho Operations Office Contract DE-AC07-0SID14517. [Online]. Available: <https://www.nrc.gov/docs/ML1822/ML18228A779.pdf>
- [14] W. Moe, "Licensing modernization project for advanced reactor technologies: FY 2018 project status report."
- [15] F. Ho, R. Vollmar, and R. Turner. Graphite design handbook. [Online]. Available: <https://www.osti.gov/servlets/purl/714896/>
- [16] M. El-Genk and T. Schriener. Post-operation radiological source term and dose rate estimates for the scalable LIquid metal-cooled small modular reactor | elsevier enhanced reader. [Online]. Available: <https://reader.elsevier.com/reader/sd/pii/S0306454918300550?token=72A5D70FC4A85A4EF41A5E9256B0B120D6DBE8E80266F7BFD35BB528A887F463F8647F134921742AAE435B0A9D635F61>

- [17] Accuratus. Silicon carbide SiC material properties. [Online]. Available: <https://www.accuratus.com/silicar.html>
- [18] W. Johnson and G. Engle, "Properties of unirradiated fuel element graphites h-451 and TS-1240," pp. GA-A-13 752, 7 283 150. [Online]. Available: <http://www.osti.gov/servlets/purl/7283150-NEjJgM/>
- [19] M. B. Richards, "Reaction of nuclear-grade graphite with low concentrations of steam in the helium coolant of an MHTGR," vol. 15, no. 9, pp. 729–739. [Online]. Available: <http://www.sciencedirect.com/science/article/pii/036054429090112F>
- [20] S. G. Nagley, C. M. Barnes, D. L. Husser, M. L. Nowlin, and W. C. Richardson, "Fabrication of uranium oxycarbide kernels for HTR fuel," p. 10.
- [21] "Accident analysis for nuclear power plants with modular high temperature gas cooled reactors," OCLC: 637106283.
- [22] M. Rainer, "Fission product transport and source terms in HTRs: Experience from AVR pebble bed reactor," vol. 2008.
- [23] E. Eaves, "Can north america's advanced nuclear reactor companies help save the planet?" vol. 73, no. 1, p. 27. [Online]. Available: <http://search.ebscohost.com/login.aspx?direct=true&db=ulh&AN=120392537>
- [24] M. Englert, F. Frieß, and M. V. Ramana, "Accident scenarios involving pebble bed high temperature reactors," vol. 25, no. 1, pp. 42–55. [Online]. Available: <https://www.tandfonline.com/doi/full/10.1080/08929882.2017.1275320>
- [25] Y. Brits, F. Botha, H. van Antwerpen, and H.-W. Chi, "A control approach investigation of the xe-100 plant to perform load following within the operational range of 100 – 25 – 100%," vol. 329, pp. 12–19. [Online]. Available: <http://www.sciencedirect.com/science/article/pii/S0029549317305630>
- [26] ESPI Metals. Graphite-pyrolytic grade. [Online]. Available: <https://www.espimetals.com/index.php/technical-data/74-graphite-pyrolytic-grade>
- [27] M. V. Ramana, "The checkered operational history of high-temperature gas-cooled reactors," vol. 72, no. 3, pp. 171–179. [Online]. Available: <https://doi.org/10.1080/00963402.2016.1170395>
- [28] Z. Zhang and Y. Sun, "Economic potential of modular reactor nuclear power plants based on the chinese HTR-PM project," vol. 237, no. 23, pp. 2265–2274. [Online]. Available: <http://www.sciencedirect.com/science/article/pii/S002954930700283X>
- [29] H. Reutler and G. H. Lohnert, "Advantages of going modular in HTRs," vol. 78, no. 2, pp. 129–136. [Online]. Available: <http://www.sciencedirect.com/science/article/pii/002954938490298X>
- [30] G. W. Helmreich, J. D. Hunn, J. W. McMurray, R. D. Hunt, B. C. Jolly, M. P. Trammell, D. R. Brown, B. J. Blamer, T. J. Reif, and H. T. Kim, "Year one summary of x-energy pebble fuel development at ORNL." [Online]. Available: <https://www.osti.gov/biblio/1376502>
- [31] M. Hussain, F. Reitsma, M. Subki, and H. Kiuchi, "Advances in small modular reactor technology developments." [Online]. Available: <http://aris.iaea.org>
- [32] B. Harlan, "ANS xe 100 overview 2017." [Online]. Available: http://local.ans.org/dc/wp-content/uploads/2014/01/ANS_Xe-100-Overview_04052017.pdf
- [33] H. G. Hereward, H. R. Paneth, G. C. Laurence, and B. W. Sargent, "Measurement of the diffusion length of thermal neutrons in graphite," vol. 25a, no. 1, pp. 15–25, publisher: NRC Research Press. [Online]. Available: <https://www.nrcresearchpress.com/doi/abs/10.1139/cjr47a-002>
- [34] E. Mulder, "Reactor physics overview of the xe-100 GEN IV reactor," NPREG 596 Graduate Seminar.
- [35] R. Nanstad and W. L. Server. Milestone report-08-2011-assessment of thermal annealing-FINAL.pdf. [Online]. Available: <https://www.energy.gov/sites/prod/files/Milestone%20Report-08-2011-Assessment%20of%20Thermal%20Annealing-FINAL.pdf>

- [36] O. K. Chopra and A. S. Rao, “Degradation of LWR core internal materials due to neutron irradiation.” [Online]. Available: <https://www.nrc.gov/docs/ML1027/ML102790482.pdf>
- [37] T. Dudley, O. Tsaoi, and E. Mulder, “THE REACTOR CORE NEUTRONIC MODEL FOR THE PBMR PLANT TRAINING SIMULATOR,” p. 13.
- [38] E. J. Mulder, “Pebble bed reactor with equalised core power distribution inherently safe and simple.” [Online]. Available: <https://juser.fz-juelich.de/record/820874/>
- [39] NASA’s Goddard Institute for Space Studies, “Global surface temperature.” [Online]. Available: <https://climate.nasa.gov/vital-signs/global-temperature>
- [40] Pebble bed modular reactor SOC ltd. [Online]. Available: <http://www.pbmrv.co.za/index2.asp?Content=129>
- [41] L. Lommers and G. Honma, “NGNP high temperature materials white paper.” [Online]. Available: <https://www.osti.gov/biblio/1055953-ngnp-high-temperature-materials-white-paper>
- [42] Cole Gentry. generate random particle or pebble bed files for HTGR calc - discussion forum for serpent users. [Online]. Available: <https://ttuki.vtt.fi/serpent/viewtopic.php?f=3&t=2267&p=6161&hilit=growth+and+shake#p6161>
- [43] I. MURATA, A. TAKAHASHI, T. MORI, and M. NAKAGAWA, “New sampling method in continuous energy monte carlo calculation for pebble bed reactors,” vol. 34, no. 8, pp. 734–744, publisher: Taylor & Francis _eprint: <https://doi.org/10.1080/18811248.1997.9733737>. [Online]. Available: <https://doi.org/10.1080/18811248.1997.9733737>
- [44] T.K.Kim, W.S. Yang, T.A. Taiwo, and H.S. Khalil, “Whole-core depletion studies in support of fuel specification for the next generation nuclear plant (NGNP) core.” [Online]. Available: <https://publications.anl.gov/anlpubs/2004/11/51497.pdf>
- [45] M. Türkmen and Çolak, “Effect of pebble packing on neutron spectrum and the isotopic composition of HTGR fuel,” vol. 46, pp. 29–36. [Online]. Available: <https://www.sciencedirect.com/science/article/pii/S0306454912000953>
- [46] Z. Karriem, C. Stoker, and F. Reitsma, “MCNP modelling of HTGR pebble-type fuel,” in *Advanced Monte Carlo for Radiation Physics, Particle Transport Simulation and Applications*, A. Kling, F. J. C. Barão, M. Nakagawa, L. Távora, and P. Vaz, Eds. Springer, pp. 841–846.
- [47] F. B. Brown, W. R. Martin, W. Ji, J. L. Conlin, and J. C. Lee, “STOCHASTIC GEOMETRY AND HTGR MODELING WITH MCNP5,” p. 13.
- [48] C. J. Hamilton, N. D. Holder, V. H. Pierce, and M. W. Robertson, “HTGR spent fuel composition and fuel element block flow.” [Online]. Available: <https://www.osti.gov/biblio/7157851>